Design of Novel Biosensing Systems for Ligand Molecules by Combination of Fluorescent Unnatural Mutant Binding Proteins and Ligand Analogues

A dissertation submitted to the

Graduate School of Innovative Life Science for Education,

University of Toyama

Toyama, Japan

for the degree of

DOCTORATE OF PHILOSOPHY (Ph.D.)

in Biological Information Systems Science

March 2014

By

Xianwei Zhu

Contents

Chapter.1 Introduction, Background and Purpose.....3

1.1 Protein engineering 3

1.2 Four-base codon method for synthesis of novel functional unnatural proteins .5

1.3 Molecular biosensors 7

1.4 Mechanism of fluorescence quenching 8

1.5 The purpose of this study 23

Chapter.2 Molecular biosensor for biotin base on fluorescence quenching of fluorescent unnatural mutant streptavidin by carbazole-labeled biotin 24

2.1 Introduction 24

2.2 Experimental methods 28

2.2-1 Materials.....28

2.2-2 Synthesis of fluorescent unnatural mutant streptavidin 30

2.2-3 Synthesis of the carbazole-labeled biotin 42

2.2-4 Experimental procedure for fluorescence biosensing 43

2.3 Results and discussion 44

2.3-1 Confirmation of the synthesis of the unnatural mutant streptavidins 44

Confirmation of the biotin binding activity of the unnatural mutant streptavidins 52

2.3-2 Fluorescence analysis of the fluorescent unnatural mutant streptavidins 54

Fluorescence measure of the unnatural mutant streptavidins upon binding of carbazole-labeled biotin and free biotin 59

Chapter.3 Molecular biosensor for biotin base on fluorescence enhancement of fluorescent unnatural mutant streptavidin by a biotin analogue with spacer tail.....70

3.1 Introduction 70

3.2 Experimental methods 72

3.2-1 Experimental procedure for fluorescence biosensing 72

3.3 Results and discussion 73

3.3-1 Fluorescence measure of the unnatural mutant streptavidins upon binding of biotin-$(AC_5)_2$-hydrazide and free biotin 73

Chapter.4 Conclusion and Perspective 79

Acknowledgments 80

References.....81

Chapter.1 Introduction, Background and Purpose:

1.1 Protein engineering:

Proteins are essential parts of organisms and participate in virtually every process within cells. Many proteins are enzymes that catalyze biochemical reactions and are vital to metabolism. Proteins also have structural or mechanical functions, such as actin and myosin in muscle and the proteins in the cytoskeleton, which form a system of scaffolding that maintains cell shape. Other proteins are important in cell signaling, immune responses, cell adhesion, and the cell cycle. Otherwise, proteins perform a vast array of functions within living organisms, including catalyzing metabolic reactions, replicating DNA, responding to stimuli, and transporting molecules from one location to another [1-4].

Proteins are also applied in current biotechnologies. for example: polymerase chain reaction (PCR) technology, western blot analysis and immunohistochemistry analysis, gene cloning, gene therapy, monoclonal antibodies, cultivation and differentiation of stem cell technology. We can find protein such as enzymes, antibodies, binding protein, inducing factor and so on in these biotechnologies above mentioned. In addition, with the progress of technology and demands, natural protein is not able to meet the needs of investigators and technical workers [5-8].

Protein engineering is the process of developing useful or valuable natural and unnatural proteins. It is a very powerful technology that could be used in a large amount of fields such as biological chemistry, cytology, medical science, pharmacy, biotechnology and so on.

There are two general strategies for protein engineering, 'rational' protein design and directed evolution. Recently, some researchers change the substrate specificity by changing individual deoxynucleotide of the relative enzyme protein genes. For instance, the substrate specificity of glucose oxidase was changed by replacing the 520th and 563th histidine of glucose oxidase; also some researchers design a new unnatural protein by reprogramming several proteins. For instance, Cameleon, the detection tool for calcium ion, was assembled by the series of green fluorescent

protein (GFP), calmodulin, M13, and yellow fluorescent protein (YFP); What's more, Peter G. Schultz etc. incorporated an unnatural amino acid into proteins for synthesis of a functional unnatural protein using the amber codon [9-12].

1.2 Four-base codon method for synthesis of novel functional unnatural proteins:

The incorporation of functional unnatural amino acids into proteins is a powerful and versatile technique for designing a functional protein for biosensor and protein structural and functional analysis. A number of researchers have synthesized proteins containing unnatural amino acids at desired positions by using an amber suppression technique. Alternatively, four-base codon method, an excellent method can site-directed introduction of single or multiple functional unnatural amino acid that possessed fluorescent, oxidation-reduction to provide a new function into the protein. In this method, one or multiple four-base codons can be introduced into an assigned position of a protein gene. The full-length protein containing the unnatural amino acid could be produced when the four-base codon is successfully decoded by the unnatural aminoacyl-tRNA having the corresponding four-base anticodon. On the other hand, when the first three bases of the four-base codon are decoded as a three-base codon by a cognate naturally occurring aminoacyl-tRNA, a frame-shift occurs that causes the emergence of a stop codon resulting in the termination of peptide elongation. Therefore, the full-length protein could be obtained only when the four bases are successfully decoded as a single codon. The four-base codon method is advantageous over the amber codon suppression technique, because unnatural amino acids can be introduced with higher efficiencies. Moreover, using orthogonal four-base codons, even more than three unnatural amino acids can be introduced into single proteins (Fig.1) [13-18].

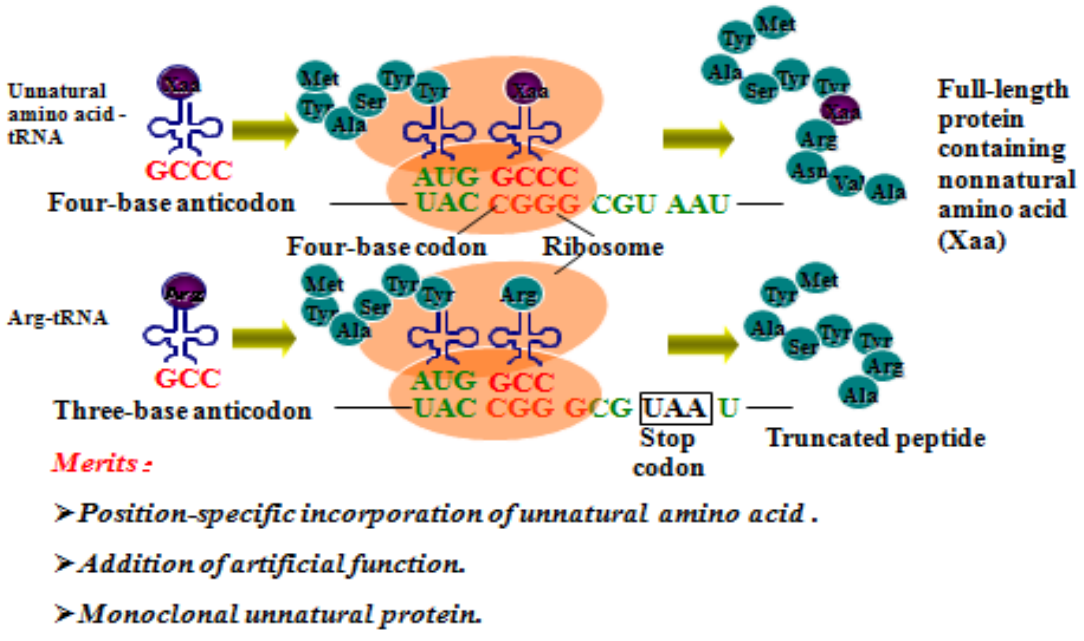

Fig.1. The mechanism of four-base codon method.

1.3 Molecular biosensors:

Biosensor is a sensor that is based on the use of biological material for its sensing function. Biosensors can be considered as a subgroup of chemical sensors in which a biological mechanism is used for analyte detection.

A biosensor is defined by the International Union of Pure and Applied Chemistry (IUPAC) as a self-contained integrated device that is capable of providing specific quantitative or semi-quantitative analytical information using a biological recognition element (biochemical receptor), which is retained in contact direct spatial with a transduction element. Biosensing systems and methods are being developed as suitable tools for different applications, including bioprocess control, food quality control, agriculture, environment, military and in particular, for medical applications. The main classes of bioreceptor elements that are applied in environmental analysis are whole cells of microorganisms, enzymes, antibodies and DNA. Additionally, in the most of the biosensors described in the literature for environmental applications electrochemical transducers are used (Fig.2) [19-24].

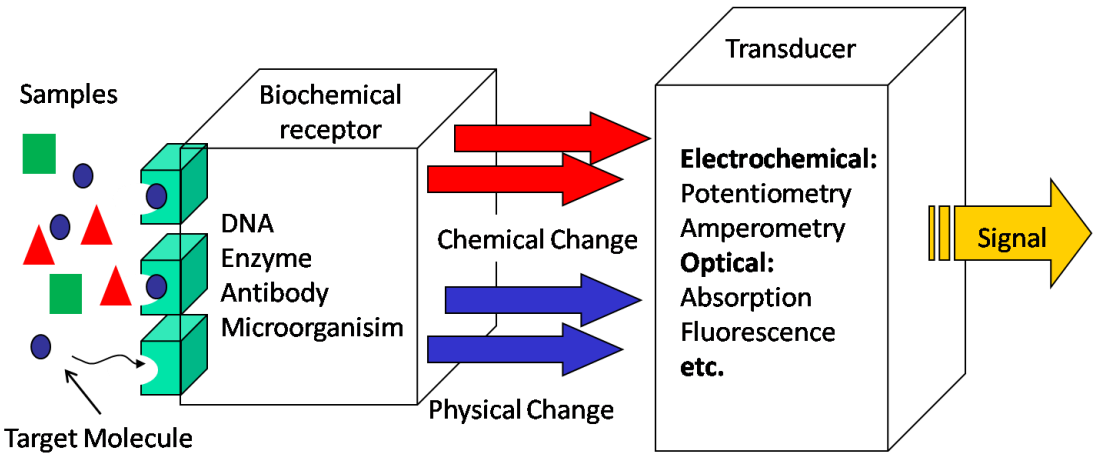

Fig.2. A schematic of a biosensor.

1.4 Mechanism of fluorescence quenching:

Fluorescence refers to photons emitted by molecules in excited states, as they return to their ground states. A fluorescence spectrophotometer measures the intensity of those photons. Quenching refers to reduction of fluorescence intensity by another molecule, one that causes some of the excited fluorescent molecule to return to their ground states without emitting photons.

As a consequence, quenching is often heavily dependent on pressure and temperature. Molecular oxygen, iodide ions and acrylamide are common chemical quenchers. The chloride ion is a well known quencher for quinine fluorescence.

Quenching is made use of in optode sensors; for instance the quenching effect of oxygen on certain ruthenium complexes allows the measurement of oxygen saturation in solution. Quenching is the basis for Förster resonance energy transfer (FRET) assays. Quenching and dequenching upon interaction with a specific molecular biological target is the basis for activatable optical contrast agents for molecular imaging.

The most commonly encountered electronic energy transfer processes in quenching phenomenon take place by two distinct type of electronic interactions between $^{*}D$ and A: case 1, the electron exchange interaction (also termed in the literature as "orbital overlap mechanism," or "electron exchange mechanism" for electronic energy transfer) and case 2, the dipole-dipole interaction (also termed in the literature as the "Coulombic," or "resonance mechanism" for electronic energy transfer). Dexter and Förster developed the theory of energy transfer induced electron exchange interactions and dipole-dipole interactions, respectively. In honor of the developers of the theories for energy transfer, electron exchange energy transfer is sometimes referred to in the literature as "Dexter" energy transfer (Fig. 3, bottom) and dipole-dipole energy transfer is sometimes referred to in the literature as "Förster" energy transfer (Fig.3, top). The overlap of frontier orbitals that is responsible for the lowest energy paths for exchange energy transfer.

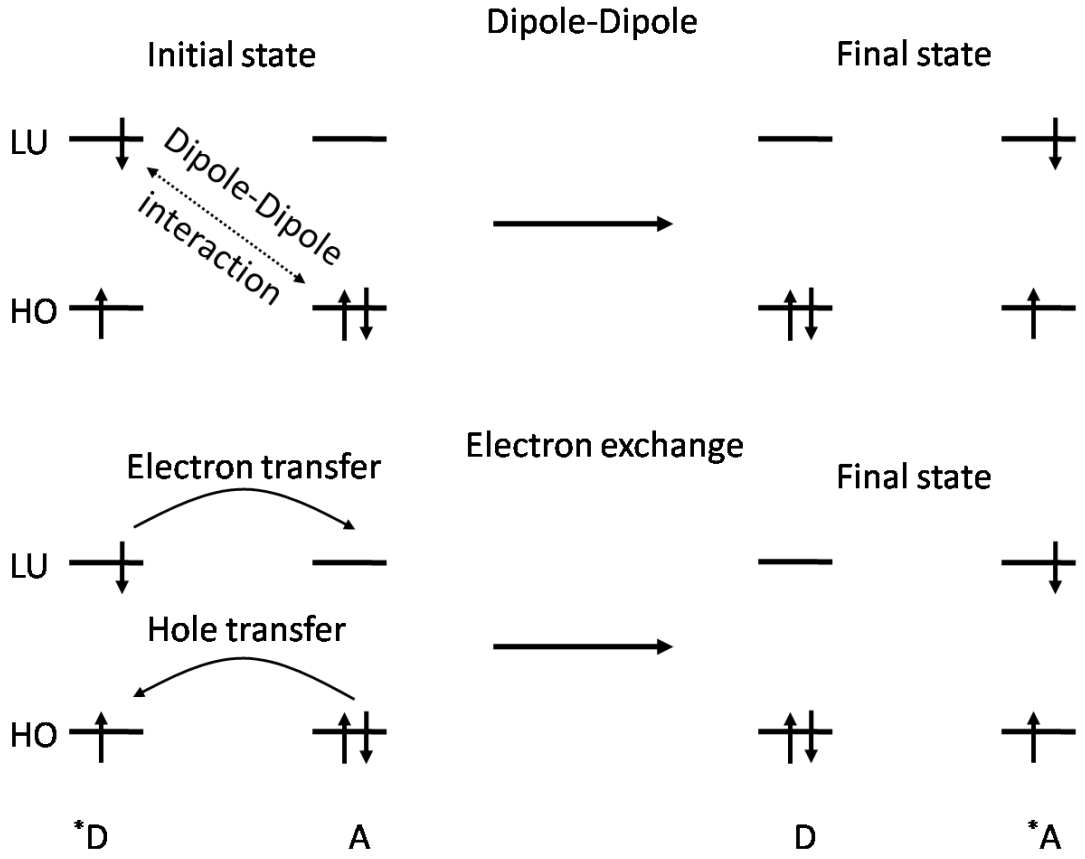

Fig.3 Comparison of the dipole-dipole and exchange mechanisms of electronic energy transfer. The spin of the electrons exchanged must obey the spin conservation rules.

In Fig.3, for bookkeeping purpose, we labeled electrons 1 and 2 as the interacting electrons. A key difference between the two mechanisms in Fig.3 is that for the dipole-dipole mechanism, the interaction between *D and A is made through space by the overlap of dipolar electric fields of *D with A, while for the exchange mechanism, the interaction between *D and A is made through the overlap of the orbitals of *D and A. The dipole-dipole interaction operates through an oscillating electron field produced by *D and does not require a van der Waals contact of *D and A or an overlap of the orbitals for *D and A. Form Fig.3 (bottom), it is seen that electrons 1 and 2 exchange positions between A and D for electron transfer; whereas from Fig.3 (top), it is seen that electron 1 stays on D and electron 2 stays on A.

For visualizing the oscillating electric field of *D which is responsible for the dipole-dipole interaction exactly. A simple pictorial model is available from the classical theory of electromagnetic radiation that views all of the electrons of a molecule as being harmonic oscillators that can undergo oscillation (similar to

electronic vibrations) along some axis on a molecular framework. In the classical model, an electron in the ground state of the harmonic oscillation does not oscillate at all in the ground state. However, *D possesses an excited electron, which according to classical theory corresponds to an excited state of the harmonic oscillator. For any excited state of a harmonic oscillator, the electron undergoes periodic harmonic oscillations along the molecular framework with a certain natural frequency (v_0). Such oscillations along the molecular framework create an oscillating electric dipole, much the same as the oscillating electric dipole for the electric field of a passing light wave. Thus, according to classical theory, *D (but not A) is imagined to possess an oscillating electric dipole that, in turn, produces an oscillating electric field in the space around *D.

The effect of this oscillating electric field of *D on a nearby A can be visualized through a familiar analogue, namely, an electrical transmitting antenna (*D) and electrical receiving antenna (A). In classical theory, A is visualized as being an initially non-oscillating electrical receiver that is potentially capable of being driven into resonance by the oscillating electric field of the transmitting antenna (*D). Suppose the frequency (v_0) at which the electron of *D oscillates matches a natural frequency for A oscillation. This condition is the first one required for resonance between *D and A. If the oscillating electric field of *D is of sufficient strength and is close enough to A to interact with A to induce oscillations of A electrons, the conditions for classical resonance and dipole-dipole energy transfer from *D to A are met. In terms of classical antennae (or tuning forks), energy flows back and forth between *D and *A. from this classical model, the energy transfer requires the existence of a common frequency of oscillation (v_0) for *D and *A. when this condition for a common frequency is met, the efficiency of energy transfer will be determined mainly by the distance of separation (R_{DA}) of *D and A, the strength of the oscillating field produced by *D at A at the separation distance, the ease at which A can be set into oscillation for the common frequency, and the relative orientation of *D and A.

According to the classical model of dipole-dipole energy transfer, electrons do not “exchange molecules or orbitals” (Fig.3 bottom), but rather the two transitions (*D → D and A →*A) occur simultaneously as resonance by which the oscillating dipole field of *D triggers the creation of a coupled oscillating dipole field about A and leads to *A. The oscillating dipoles of *D and *A are represented by the vertical doubled-headed arrows in Fig.3, top. The excitation of A to *A by the dipole-dipole mechanism is analogous to the classical mechanism for absorption of light. In the case of light absorption, the oscillating electromagnetic field of light provides the

oscillating electric dipolar field that interacts with the electrons of A. The oscillating electron of the excited molecule *D thus serves as a "virtual photon" for the production of *A. In other words, the ground state of A cannot tell whether the oscillating field that causes it to be exited to *A is due to a "real" photon from the oscillating electromagnetic field, or to the "virtual" photon from the oscillating dipolar electric field of *D.

Quantum mechanics handles both energy (electron exchange) and electron transfer in terms of interacting (overlapping) wave functions for *R and M. For any given *R and M pair, there will always be a certain degree of electron exchange interaction and dipole-dipole interaction, as they approach each other, although in general, at any given separation, one will dominate over the other. Since both the electron exchange and the dipole-dipole interaction are relatively weak, from the standpoint of quantum mechanics, electronic interactions can be analyzed in terms of the matrix elements for the interactions, as described by the golden rule for electronic transition. We can qualitatively estimate the values of the rate constants for energy transfer (k_{ET}) in terms of the corresponding matrix elements for the electron exchange and dipole-dipole interactions given by Eq.1, where α and β refer to the degree of contribution for the two interactions. According to quantum mechanics, the strength (energy) of the interaction that triggers energy transfer is directly proportional to the magnitude of the matrix element corresponding to the interaction. However, the rate of energy transfer given by k_{ET}, is proportional to the square of the strength (energy) of the interaction; therefore, k_{ET} is proportional to the square of the matrix element corresponding to the interaction.

In the case of electron exchange, the form of the operator Hex in Eq.1 is $exp(-R_{DA})$, where R_{DA} is the separation between the energy donor *D and the energy acceptor A. This mathematical form is reasonable because, in general, the magnitude of electronic wave function tend to fall off exponentially as a function of distance from a point of reference, such as a nucleus. Thus, the rate constant for energy transfer by the electron exchange interaction is expected to fall off exponentially as the separation R_{DA} between *D and A increase. In the case of dipole-dipole energy transfer, the operator H_{dd} has the form $\mu_{*_D}\mu_{*_A}/R_{DA}^3$, where μ_{*_D} is the strength of the oscillating dipole due to *D in Fig.3; μ_{*_A} is the strength of the oscillating dipole of *A; and R_{DA} is the separation of the donor and acceptor. Since the matrix element is squared in Eq.1, the rate of energy transfer by the dipole-dipole interaction will fall off as the square of $1/R_{DA}^3$ (i.e., $1/R_{DA}^6$).

$$k_{ET}(total) \propto \left\{ \begin{array}{c} \alpha[\psi(*D)\psi(A)|H_{ex}|\psi(D)\psi(*A)]^2 \\ Electron\ exchange \\ + \\ \beta[\psi(*D)\psi(A)|H_{dd}|\psi(D)\psi(*A)]^2 \\ Electron\ dipole-dipole\ interactions \end{array} \right\} \quad (1)$$

As a concrete quantitative model for the dipole-dipole interaction, we assume that the oscillating electric field near *D behaves similarly to the field generated by a classical harmonic electric oscillator antenna whose frequency of oscillation is v_0 and whose instantaneous oscillating, or transition dipole, at any instant is μ (Fig.3, top). If $|\mu_0|$ is the maximum value of the transition dipole μ that can be achieved, we apply the classical expression for the oscillating field of a harmonic oscillator (Eq.2) to determine the value of μ at any instant t:

$$\mu = \mu_0 cos(2\pi vt) \quad (2)$$

Where t is time and v is the frequency of oscillation. In molecular terms, we can identify this oscillating dipole moment as resulting from amplitude of the back-and-forth electric vibrational motion along the molecular framework of the excited electron on *D; the electric charge oscillates along the molecular framework just like the charge oscillates back and forth along the an antenna. Recall that in classical theory, for the ground state of A, the electrons are assumed not to oscillate at all (the oscillation is considered to have zero amplitude). The resulting dipolar electron-charge oscillation of *D will induce the oscillation and eventually the excitation of electronic system of nearby molecules, if the usual resonance conditions (correct frequency, finite interactions, equal energy gaps for transitions and conservation laws) are met. This dipole-dipole coupling mechanism for energy transfer is plausible only in multiplicity-conserving (spin allowed) transitions that have large transition dipoles (μ). Only singlet-singlet transitions have large oscillator strengths and are associated with large transition dipoles; therefore, only singlet-singlet energy transfer is generally plausible by the dipole-dipole mechanism. However, electron exchange provides an effective mechanism for triplet-triplet energy transfer. Thus, whenever we find an example of energy transfer from a triplet dipole interactions donor to produce a triplet acceptor, we can readily assume that electron transfer is involved. Dipole-dipole interactions ruled out as an implausible mechanism for energy transfer since neither the donor *D, nor the acceptor A, possess significant transition dipoles, so that the dipole-dipole interaction will be very weak.

For the radiative transition, the resonance condition (energy of transition is equal to the energy for a photon of frequency, *v*) is given by Eq.3.

$$\Delta E(A \rightarrow * A) = hv \qquad (3)$$

The energy conservation is an absolute requirement for energy transfer by any mechanism. For molecules, the matching of the energy for the *D→D and A→*A transitions will generally involve matching of vibrational energy levels. Since *D will be in its lowest vibrational level (*v=0*), we see that an excited vibrational level of *A will be produced by the energy-transfer process of Eq.4.

$$\Delta E(* D \rightarrow D) = \Delta E(A \rightarrow * A) \qquad (4)$$

Since the resonance condition must e met from Eq.4, we can deduce the common frequency of oscillation, since $\Delta E = hv$ so $v = \Delta E/h$.

Förster pointed out that in classical theory the electrostatic interaction energy (*E*) between two electric dipoles is directly related to the magnitude of the two interacting dipole (μ_D and μ_A, Eq.2) and inversely related to the cube of the distance between the donor and acceptor (R_{DA}), as shown in Eq.5.

$$Electrostatic\ interaction\ energy$$
$$E\ (dipole - dipole)\ \propto \frac{\mu_D \mu_A}{R_{DA}^3} \qquad (5)$$

From Eq.5, we see that the key parameters determining the energy (strength)of the dipole-dipole interaction are the size of the interacting dipoles μ_D and μ_A and the cube of their separation R_{DA} .Förster related the electric dipoles (μ_D and μ_A) to the oscillator strength (f_D *and* f_A) for radiative *D↔D and A↔*A transitions, respectively. Recall that the theoretical quantities f_D *and* f_A are related to the experimental extinction coefficients ε_D and ε_A. The oscillator strength (*f*) for the interaction of the electromagnetic field and the electrons of a molecule is based on the model of an idealized harmonic oscillator for both the oscillating electric field of a light wave and the oscillating electron for an electronically excited state. The energy (*E*) of classical dipole- dipole interaction can be formulated in terms of f_D *and* f_A (the oscillator strengths are measurable through extinction coefficients, ε) for the radiative transitions of *D→D and A→*A. Now we can see how factors that control the strengths of electronic radiative transitions also control the strength of dipole

interactions in dipole-dipole energy transfer at any fixed distance of separation (R_{DA}). A final theory for energy transfer by the dipole-dipole interaction for real systems must include electronic, vibrational, and spin factors in addition to solvent dielectric factors (dipole-dipole interactions are dependent on the dielectric constant of the surrounding medium).

$$k_{obs} \sim \rho[\langle\psi_1|p'_{1\to2}|\psi_2\rangle]^2 \qquad (Fermi's golden\ rule) \qquad (6)$$

Quantum mechanical principles can be applied to Eq.1 to modify the classical models as follows. Since the dipole-dipole interactions are weak electronic interactions, the quantum mechanical golden rule for electronic transitions (Eq.6), which may be applied to all weakly interactive systems, can be used to compute the rate of energy transfer (k_{ET}) by the dipole-dipole mechanism as shown in Eq.7. The matrix element (for the form of Eq.1) for energy-transfer process *D+A→D+*A involves the product wave function ($\Psi(*D)\Psi(A)$) for the initial state, the product wave function ($\Psi(D)\Psi(*A)$) for the final state, and an operator $P_{D\to*A}$ that corresponds to dipole-dipole interaction of Eq.7, which mixes the wave functions $\Psi(*D)$ and $\Psi(A)$ of the initial state and causes transition to the wave function of the final states $\Psi(*D)$ and $\Psi(A)$. According to the golden rule, the value of the rate constant for energy transfer (k_{ET}) depends on the square of this matrix element (Eq.7). In addition, there is a term ρ that is a measure of the "density of state" that have the same energy in *D and A and that are also coupled by the dipole-dipole interaction. This set of "overlapping states" of *D and A can be expressed quantitatively as an "overlap integral" whose value is given by ρ. In addition, the golden rule can be conveniently formulated as a product of the square of an electronic matrix element and the square of the Franck-Condon (FC) factors for the energy conserving transitions (Eq.8).The term $\langle X_i|X_f\rangle$ is related to term ρ and is the FC factor. This latter term is important because it shows that simply conserving energy and having good positive overlap of the electronic wave function is necessary, but not sufficient, for an energy transition to be probable. In addition, the states involves in the energy transfer must have good positive overlap for the vibrational wave function of the initial state (X_i) and the vibrational wave function of the final state (X_f) .(The spin wave function, of course, is also important, but is ignored at this point for simplicity).

$$k_{ET} \sim \langle\psi(*D)\psi(A)|P_{D\to*A}|\psi(D)\psi(*A)\rangle^2\rho \quad Golden\ rule \qquad (7)$$

$$k_{ET} \sim \langle\psi(*D)\psi(A)|P_{D\to*A}|\psi(D)\psi(*A)\rangle^2\langle X_i|X_f\rangle^2 \qquad (8)$$

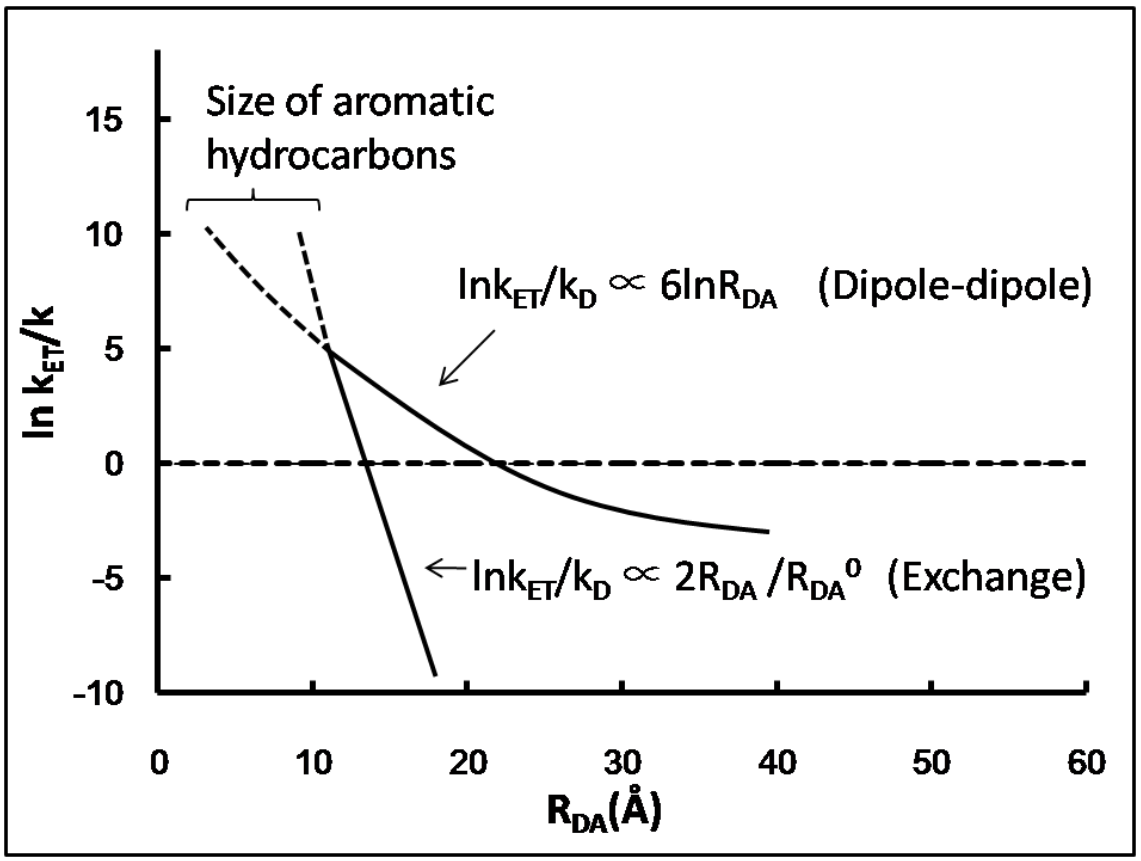

Fig.4 Hypothetical graphs of the rate ratio of energy transfer (k_{ET}) to decay of *D (k_D) plotted as lnk_{ET}/k_D versus $6lnR_{DA}$ (dipole-dipole energy transfer) and versus $2R_{DA}/R_{DA}^0$ (exchange energy transfer).

From this analysis, we conclude that in general the magnitude of k_{ET} will be proportional to the square of the interaction energy, as shown in Eq.9. A poor vibrational, FC factor, or a change in multiplicity will lead to small interaction energy because poor FC factors or changes in spin correspond to small transition dipole moments. Recall that oscillator strength is related to the inherent radiative lifetime and the extinction coefficient of a given transition. By applying the golden rule (Eq.7), k_{ET} (dipole-dipole) is related to E^2 quantitatively through Eq.9. Note from Eq.9 that the rate of dipole-dipole energy transfer (assuming point dipoles) falls off as the inverse sixth power of the separation of the dipoles (R_{DA}) .Thus, the rate of electronic transfer is expected to fall off as the separation (R_{DA}) between *D and A increases, by a factor of $1/R_{DA}^6$. This $1/R_{DA}^6$ distance dependence, when it can be measured accurately, is a basis for distinguishing energy transfer that occurs by dipole-dipole interactions from electron exchange interactions, since the latter generally falls off exponentially with the separation R_{DA}. An exemplar that compares the dependence for rate of energy transfer by the dipole-dipole and by the electron exchange mechanism is shown in Fig.4, where the falloff of lnk_{ET} compared to deactivation

of the donor (k_0) is given as a function of separation of *D and A (R_{DA}). In this exemplar, it is seen that for relatively small separations (*<10 Å*) for both interactions the rate of energy transfer is $\gg k_0$, and is therefore very efficient. However, for values of R_{DA}*>10Å*, the exponential falloff for the rate of energy transfer by the change mechanism (a linear falloff since In is being plotted) is generally steeper than the $1/R^6$ falloff of the dipole-dipole interaction. Consequently, in the hypothetical exemplar example shown, even at values of $R_{DA} \sim$*30-40Å* dipole-dipole energy transfer and decay of *D are still competitive, but the energy transfer by electron exchange is not significant. This example shows that in favorable cases the range of separations for *D and A energy transfer by the dipole-dipole mechanism can be much large than (*>30Å*) the size of typical organic molecules (*5-10Å*).

$$k_{ET}(Dipole-dipole) \propto E^2 \approx \left(\frac{\mu_D \mu_A}{R_{DA}^3}\right)^2 = \frac{\mu_D^2 \mu_A^2}{R_{DA}^6} \qquad (9)$$

In summary, from Eq.9, Förster theory predicts that k_{ET} for an energy transfer via dipole-dipole interactions will be proportional to the following quantities:

1. The square of the transition dipole moment μ_D, corresponding to the *D→D transition
2. The square of the transition dipole moment μ_A corresponding to the A→*A transition.
3. The inverse sixth power of the separation between *D and A (*i.e.,* $1/R_{DA}^6$).

Förster related the theoretical quantities of oscillator strength (*f*) and transition dipole (μ) to experimental quantities, such as extinction coefficients (ε) or radiative lifetime (k^0). The relationships are between the transition moments and experimental quantities ε and k^0. From these relationships, we deduce that a direct proportionality exists (Eq.10 and Eq.11) between μ^2 and ε (or k^0):

$$\mu_D^2(D^* \leftrightarrow D) \rightarrow \int \varepsilon_D \; or \; \int k_D^0 \qquad (10)$$
$$\mu_A^2(A^* \leftrightarrow A) \rightarrow \int \varepsilon_A \; or \; \int k_A^0 \qquad (11)$$

Where $\int \varepsilon$ represents an integration of the experimental extinction coefficient for an absorption band over energy and $\int k^0$ represents an integration of the pure radiative rate constant over an emission band.

Since we are specifically considering an energy-transfer process for the simultaneous coupled transitions *D→D and A→*A, we select k_D^0 and $\int \varepsilon_A$ as the relevant experimental terms to replace the square of the theoretical transition dipole

moments of Eq.10 and Eq.11 and obtain Eq.12, which relates k_{ET} to experimentally measurable quantities, k_D^0 and $\int \varepsilon_A$, as a function of the separation of R_{DA}.

$$k_{ET}(\text{dipole} - \text{dipole}) = \alpha \frac{k_D^0 \int \varepsilon_A}{R_{DA}^6} \quad (12)$$

Finally, the value of k_{ET} also depends on the spectral overlap requirement. By considering the overlap of *D emission with A absorption, we obtain Eq.7.29, from which values of k_{ET} can be computed from experimental data.

$$k_{ET}(dipole - dipole) = \alpha \frac{\kappa^2 k_D^0}{R_{DA}^6} J(\varepsilon_A) \quad (13)$$

The term α in Eq.12 and Eq.13 is a proportionality constant determined by experimental conditions, such as concentration and solvent index of refraction. The term κ^2 takes into account the fact that the dipoles μ_D and μ_A are vector quantities, and that the interaction between two oscillating dipole vectors will depend on the mutual orientation of the dipoles in space. For a random distribution of orientations for dipoles in space from geometric considerations, κ^2 turns out to be a constant equal to two-thirds. The term $J(\varepsilon_A)$, the spectral density integral, is a quantity that is similar to the overlap integral of Eq.14, except that the value of the extinction coefficient of the acceptor(ε_A) is included in the integration. A large value of ε_A means that A has a large oscillatory strength and can readily be set into resonance to from *A. The spectra density integral is related to the density of states (ρ) in the golden rule expression(Eq.8). We include ε_A because the number of states for the same energy, which is given by the normalized overlap integral, is important, as is the dipole-dipole interaction of each isoenergetic *D and A transition (FC factors in Eq.8). The strength of the interactions for these isoenergetic transitions requires inclusion of the oscillator strength for the acceptor or ε_A. The inclusion of k_D^0, the inherent radiative lifetime of *D, takes into account the strength of the transition dipole for the energy donor since k_D^0 is proportional to the oscillator strength of the radiative *D→D+hv transition.

From Eq.13, we can anticipate that the conditions for which the rate constant of energy transfer from *D to A, induced by the dipole-dipole mechanism, will be maximal when:

1. The *D→D and A→*A transitions correspond to a large (spectral) overlap integral, $J(\varepsilon_A)$. A large value of $J(\varepsilon_A)$ means that there are many resonant *D→D

and A→*A transitions, that is, there is a high "density of isoenergetic states" ρ, in the golden rule equations Eq.6 and Eq.7.

2. The radiative rate constant (k_D^0) is as large as possible $k_D^0 = (\tau_D^0)^{-1}$. A large value of k_D^0 means that the *D→D transition possess a large oscillator strength (f), which in turn means that that the size of the oscillating transition dipole (μ_D) due to the excited electron of *D is very large and is a strong oscillator. Therefore, the dipolar field generated by *D in the space around its vicinity is large. Now, *D is a strong and effective transmitting antenna for inducing the oscillation of accepting dipoles in the space around it when the resonance conditions are met.
3. The magnitude of ε_A is as large as possible in the overlap region. A large valve of ε means that the A→*A transition possess a large oscillator strength, which in turn means that the size of the oscillating dipole (μ_A) is large and that A is a good antenna for receiving dipole oscillations, if the resonance condition is met.
4. The spatial separation (R_{DA}) between *D and A is smaller than the critical separation required for efficient energy transfer. In actual applications, it is convenient to define a specific critical average separation (R_{DA}^0) for which the rate of electronic energy transfer from *D to A is equal to the rate of deactivation for *D; that is, $k_0 = k_{ET}[A]$. When $R_{DA} < R_{DA}^0$, most of the *D molecules will be deactivated by energy transfer, and when $R_{DA} < R_{DA}^0$ energy transfer becomes inefficient. Pictorially, the closer *D is to A, the stronger is its oscillating force field felt by A, and therefore the more powerful its interaction with A.
5. For a given separation for which *D is interacting with A, there will be preferred relative orientations of *D and A for which energy transfer is favorable and fast, and other orientations for which energy is unfavorable and slow. Recall that the interaction energy between two dipoles. Thus, for certain orientations the interaction will be small, even if *D and A are very close to one another, that is, closer than the average separation (R_{DA}^0) .Indeed, near the "magic angle" of θ∼ 54°, the dipole-dipole interaction is close to zero and both have large transition dipoles, no matter how close the dipoles are in space(within the point dipole approximation).We can see that for a detailed computation, we must consider not only the "center-to-center" separation of R_{DA}^0 (based on a simple spherical model)but also the orientation of the dipoles of *D and A.

Experimentally, it is often more convenient to measure the efficiency of energy transfer (φ_{ET}) rather than the rate constant of energy transfer (k_{ET}) since φ_{ET} depends only on the spatial separation R_{DA} between *D and A for a given *D and A pair that are randomly separated in space. Conceptually, the efficiency of energy transfer φ_{ET}

provides information on the fraction of initial *D molecules that succeed in transferring energy to the acceptor A. As mentioned in condition, it is convenient to define a separation R_{DA} for which the rate of energy transfer equals the sum of the rates for deactivation of *D, as shown in Eq.15 and Eq.16, where k_D is the reciprocal of the experimental lifetime of *D under the conditions of the experiment and for which *[A] = 0*.Note that k_D is not the inherent radiative lifetime k_D^0 that corresponds to the situation for which where is no radiationless deactivation of *D. When Eq.15 is valid, since the rate of energy transfer from *D to A and the rate of deactivation of *D are equal, 50% of *D id quenched by electronic energy transfer to A and 50% of *D is quenched by the processes that deactivate *D in the absence of A. The distance at which Eq.7.30a is valid is termed the "critical separation distance" (R_{DA}^0) .

$$J = \int_0^\infty I_D(\nu')\varepsilon_A(\nu')d\nu' \qquad (14)$$

$$k_{ET}[*D][A] = k_D[*D] \quad at \quad R_{DA} = R_{DA}^0 \qquad (15)$$

or

$$k_{ET}[A] = k_D = \tau_D^{-1} \qquad (16)$$

Note that in Eq.16, k_D and τ refer to the experimental rate constant for total decay and lifetime of *D, respectively. The actual lifetime of *D under most experimental conditions will normally be shorter than the radiative lifetime τ_D^0 [recall from Eq.19 that $\tau_D^0 = (k_D^0)^{-1}$], since generally radiationless processes will compete with radiative processes for the deactivation of *D. The efficiency of emission from *D is related to the measured and radiative lifetimes by Eq.17.

$$\phi_{emission} = \frac{\tau_D}{\tau_D^0} \qquad (17)$$

When [A] is such that the equality of Eq.15 is found experimentally, we may calculate R_{DA}^0, the average separation for *D and A for which energy transfer and deactivation of *D occur at equal rates. Taking into account geometric factors and assuming spherical shapes for D and A, the relationship between R_{DA}^0 and the concentration $[A]_0$ that meets the criteria of Eq.15 is given by Eq.18.

$$R_{DA}^0(in\text{Å}) = 6.5[A]^{1/3} \quad with\ [A]\ in\ M\ units \qquad (18)$$

The rate constant and the efficiency for energy by the dipole-dipole mechanism may then be related to the actual separation R_{DA} of *D and A by Eq.19 and Eq.20,

respectively.

Rate constant for any separation:

$$k_{ET} \propto k_D \left(\frac{R_{DA}^0}{R_{DA}}\right)^6 = \frac{1}{\tau_D}\left(\frac{R_{DA}^0}{R_{DA}}\right)^6 \quad (19)$$

Efficient for any separation:

$$\phi_{ET} \propto \left(\frac{R_{DA}^0}{R_{DA}}\right)^6 \quad (20)$$

In Eq.19, τ_D is the experimental lifetime of *D, R_{DA} is the actual separation between centers of *D and A, R_{DA}^0 is the critical separation as defined by Eq.15, and ϕ_{ET} is the efficiency for energy transfer (Eq.21). Thus, when $R_{DA} = R_{DA}^0$, the rate of energy transfer equals the rate of deactivation (Eq.15 and Eq.16). When $R_{DA} < R_{DA}^0$, energy transfer predominates, whereas when $R_{DA} > R_{DA}^0$ deactivation of *D dominates.

Forster resonance energy transfer (commonly termed FRET)is widely used in photobiology as a ruler to determine distances between chromophores, sometimes strategically placed to examine special features or conformations in biomolecules. This interest has led to the determination of numerous R_{DA}^0 values for selected donor-acceptor pairs. Typical values of R_{DA}^0 are in the 10-50-Å range.

Bimolecular chemical interactions are usually viewed as occurring via collisions between molecular reaction partners. By collisions, we mean that the participants in the reaction are sufficiently close that their electron clouds overlap significantly (the separation of the colliding partners is slightly smaller than their van der Waals radii). In any region of orbital overlap, electron exchange always occurs. The following processes of interest to photochemists can result from electron exchange interactions produced by molecular collisions:

1. Triplet-triplet energy transfer.
2. Singlet-singlet energy transfer.
3. Triple-triple annihilation.
4. Electron transfer.

For the simple case of two spherical orbitals of *D and A, the overlap between the orbitals falls off exponentially as the separation R_{DA} between *D and A increases. This

exponential falloff is a characteristic distance dependence of orbital overlap. Since the degree of exchange for energy transfer is directly related to the orbital overlap of *D and A, the rate constant for exchange energy transfer (k_{ET}) is also expected to fall off as an exponential function of the distance separating *D and A. In addition to the dependence of the rate of exchange energy transfer on the separation of *D and A, the rate of energy transfer will also be directly related to J, the spectral overlap integral, which, as expected from the golden rule for energy transfer between states (Eq.7), is a measure of the number of states that are capable of satisfying the resonance condition, once *D and A are coupled by the electron exchange interaction as the result of finite orbital overlap. The rate constant of energy transfer by electron exchange id given by an equation of the form of Eq.22:

$$\phi_{ET} = \phi_{*D}\varphi_{ET} \quad (21)$$

$$k_{ET}(exchange) = KJ\ exp(-2R_{DA}/R_{DA}^{0}) \quad (22)$$

Where *K* is a parameter related to the specific orbital interactions, such as the dependence of orbital overlap on the instantaneous orientations of *D and A. The parameter J is the normalized spectral overlap integral (Eq.14), where normalized means that both the emission intensity (I_D) and extinction coefficient (ε_A) have been adjusted to unit area on the wavenumber (ν') scale. It is important to note that J, because it is normalized, does not depend on the actual magnitude of ε_A. This difference is an important distinction from the situation for dipole-dipole energy transfer for which the magnitude of ε_A is a direct factor in determining the overall value of J (Eq.13). The overlap integral *J* can be identified with ρ, the density of degenerate states that couple *D and A (Eq.6 and Eq.7).

Equation 26 is a convenient expression of the distance dependence for the rate constant for energy transfer by electron exchange, k_{ET}. The parameter R_{DA} is the separation of *D and A; R_{DA}^{0} is the separation of *D and A when they are in van der Waals contact; and k_0 represents the rate of energy transfer when *D and A are van der Waals contact (when $R_{DA} = R_{DA}^{0}$, then or Eq.22, $exp[-\beta(R_{DA} - R_{DA}^{0}) = 1]$). The β term in Eq.22 is a parameter that represents the sensitivity of k_{ET} to a distance of separation (R_{DA}) for a given *D and A pair. Typical values of β are on the order of $1Å^{-1}$ and generally do not depend significantly on the electronic characteristics of *D and A when energy transfer is exothermic. This finding means that the rate constant for energy transfer falls off by $\sim 1/e$ as the value of R_{DA} increases by $1Å$. Values of $\beta < 1$ mean that β is not very sensitive to separation; for small values of β, energy transfer can occur over very large distances. The maximum value of k_0 is

expected to be on the order of $10^{13}s^{-1}$. From Eq.23, for $k_0 = 10^{13}s^{-1}$, the rate of energy transfer is $10^{13}s^{-1}$when *D and A collide and are in contact; that is, $R_{DA} = R_{DA}^0$.

$$k_{ET} \sim k_0 \exp[-\beta(R_{DA} - R_{DA}^0)] \quad (23)$$

In comparing dipole-dipole interactions and electron exchange energy-transfer processes, we note the following differences in their characteristics.

1. The rate of dipole-induced energy transfer decreases as $1/R_{DA}^6$, whereas the rate of exchange-included transfer decreases as $exp(-R_{DA}/R_{DA}^0)$. Quantitatively, this means that k_{ET} (exchange) drops to negligibly small values (relative to the lifetime of *D)as the intermolecular distance between *D and A increases to values that are more than one or two molecular diameter(5-10 Å) ,as shown in Fig.4.
2. The rate of dipole-induced transfer depends on the extinction coefficients (ε) of the *D→D and A→*A radiative transitions, but the rate of the exchange-induced transfer is independent of the extinction coefficients of the *D→D and A→*A transitions.
3. The efficiency of energy transfer (fraction of transfer per donor lifetime ~ k_{ET}/k_D) by the dipole mechanism depends mainly on the oscillator strength of the A→*A transition(since a small extinction coefficient for the *D→D transition is compensated for by a slower radiative rate constant)and is directly related to the quantum yield for emission of *D, whereas the efficiency of energy transfer by the exchange interaction cannot be as directly related to experimental quantities.
4. Both Förster and Dexter theories predict a direct dependence of k_{ET} on *J*, the spectral overlap integral, but the Forster theory includes the extinction coefficient of the A→*A transition in the computation of *J* [25-32].

1.5 The purpose of this study:

In this study, two types of molecular biosensor models for small ligand molecule were investigated. The pair of Streptavidin and biotin that was used as the model was investigated here. The two types of molecular biosensor models were successfully designed by fluorescent mutant Streptavidin using fluorescence quenching mechanism and fluorescence mechanism.

Chapter.2 Molecular biosensor for biotin base on fluorescence quenching of fluorescent mutant streptavidin by carbazole-labeled biotin

2.1 Introduction:

Biotin is a water-soluble vitamin, also known as Vitamin B-7 or Vitamin H. It is the essential component for synthesis of Vitamin C, and also works as a coenzyme for the synthesis of fatty acids, isoleucine, and valine, and plays a role in gluconeogenesis. Biotin deficiency induces hair loss (alopecia), conjunctivitis, dermatitis likes a scaly red rash around the eyes, nose, mouth, and genital area, neurological symptoms like depression, lethargy, hallucination, and numbness and tingling of the extremities. Therefore, a rapid convenient method for determining the biotin concentration is very important [33-37].

Streptavidin is a tetrameric biotin binding protein isolated from *Streptmyces avidinii.* The dissociation constant (Kd) of streptavidin to biotin is on the order of 10^{-15}mol/L that is extraordinarily high affinity. Then streptavidin-biotin binding reaction has been widely applied to biotin detection, biomolecule purification, protein assays, diagnostics, and drug delivery by coupling with various reporter probes, such as fluorescence dyes, radioactive elements or enzymes. Therefore, more rapid convenient methods for the determination of biotin are further required (Fig.5a, b) [37-41].

In this study, a fluorescent unnatural amino acid, BODIPY-FL-Aminophenylalanine (BFLAF) (Fig.5c) in which BODIPY-FL was bound to aminophenylalanine was incorporated at the Tyr54, Tyr83 and Trp120 of a streptavidin to synthesize three different monoclonal fluorescent mutant streptavidin by using four-base codon method and to apply them into molecular biosensor for biosensor. On the other hand, carbazole was modified to biotin as a quencher for BFLAF. The fluorescent mutant streptavidin of Trp120BFLAF was certainly quenched by carbazole-labeled biotin (Fig.5d) when the streptavidin-biotin complex was formed. Whereas, in the presence free biotin was existed in the assay solution, the fluorescent mutant

streptavidin of Trp120BFLAF would not be quenched by carbazole-labeled biotin because of the competitive binding reactions of natural biotin and carbazole-labeled biotin to the mutant streptavidin [42-45].

By this competitive binding assay, free biotin was determined in the concentration range of 20 nM to 100 nM. This result demonstrated that various molecular biosensing systems for small ligands could be constructed by coupling the position-specifically designed fluorescence mutant binding protein and the corresponding quencher-labeled ligand analogue.

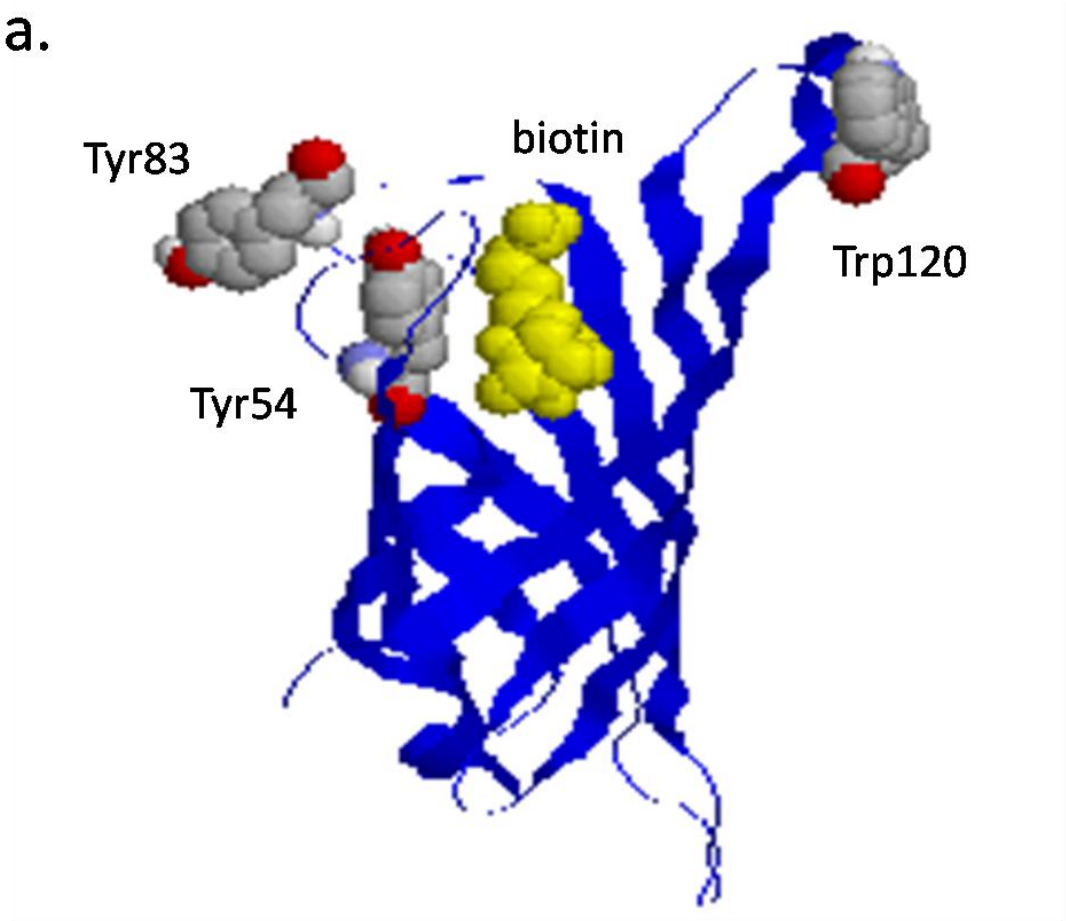

b.

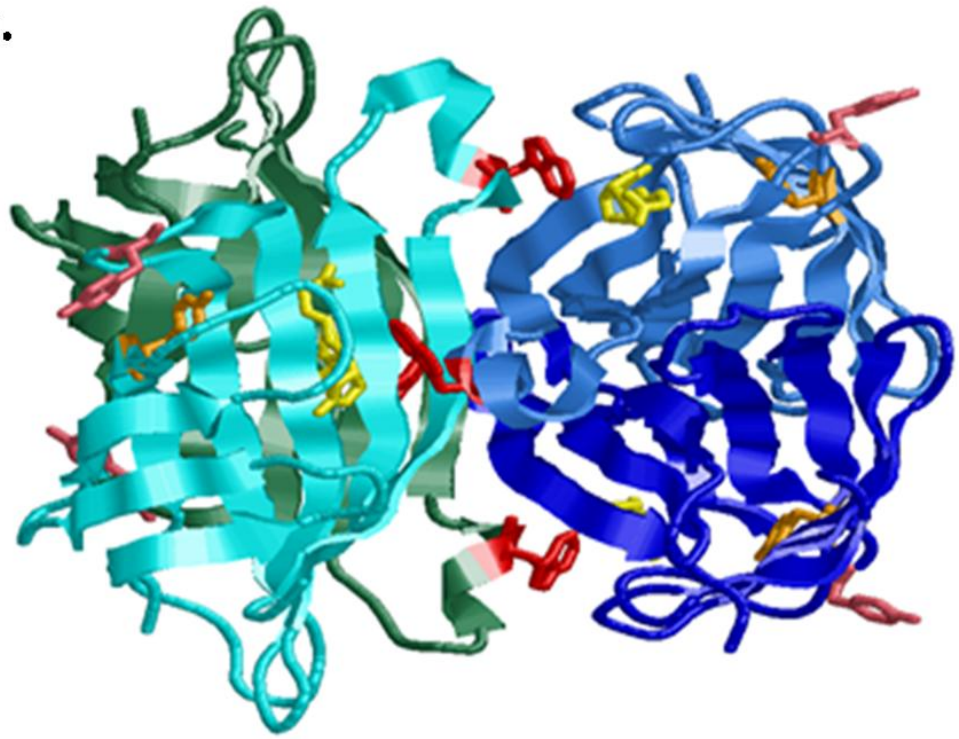

c.

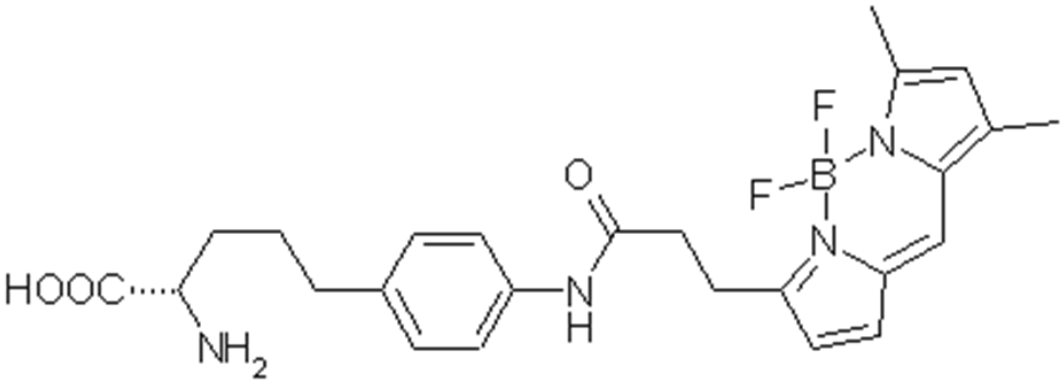

d.

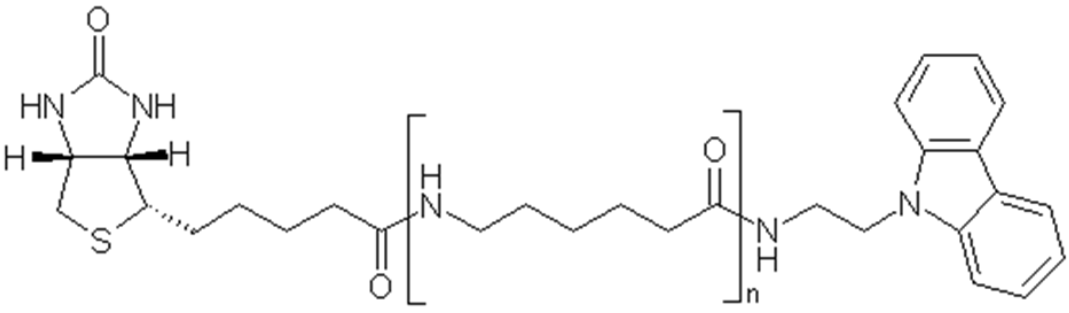

Fig.5 (a) The monomeric constitution of streptavidin.
(b) The tetrameric constitution of streptavidin. Tyr54's were colored with orange, Tyr83's were colored with pink, Trp120's were colored with red, the biotins were colored with yellow. As shown in the Fig.1a, the biotins were close to the Trp120's of the neighbor streptavidin in the streptavidin-biotin complex.
(c) Structure of BODIPY-FL-Aminophenylalanine (BFLAF) λ_{exmax}=505 nm λ_{emmax}=514 nm
(d) Structure of carbazole-labeled biotin (n=0 carbazole-labeled biotin; n=1 carbazole-LC-biotin; n=2 carbazole-LC-LC-biotin).

2.2 Experimental method:

2.2-1 Materials:

The DNAs of wild type and Tyr83, Trp120 mutant streptavidin, and DNA of the tRNA that having four-base anticodon and BODIPY-FL-Aminophenylalanyl-pdCpA were obtained from laboratory of Prof. Hohsaka of Japan advanced institute of science and technology (JAIST).

The materials for the PCR and purification of the wild type and mutant streptavidins template DNAs of mRNA and tRNA:

Vent DNA polymerase was obtained from New England Biolabs. Primers for the PCR of template DNAs of mRNA (T7 up and T7 term) and tRNA (M3 and -CA) were purchased from Sigma life science. PCR purification kit (QIAquick®) for DNAs of mRNA and PCR purification kit (MinElute®) for DNAs of tRNA were from QIAGEN.

T7 up (5'-CCCGCGCGTTGGCCGATTCA-3')

T7 term (5'-TATTACGCCAGGTTATCCGG-3')

M3 (5'-GTTGTAAAACGACGGCCAGT-3')

-CA (5'-GTGCGAATTCTGTGGATCGA-3')

The materials for the synthesis and purification of the wild type and mutant streptavidins the mRNAs and tRNA:

Thermo T7 RNA polymerase and ribonuclease inhibitor were obtained from TOYOBO. Thermostable inorganic pyrophosphatase was purchased from New England Biolabs. T4 RNA ligase was from Takara Bio.

The materials for the synthesis and purification of the wild type and mutant streptavidins:

E.coli S30 Extract system and MagneHis™Ni-Particles were purchased from Promega. G-25 columns were obtained from GE Healthcare.

The materials for the Western blotting analysis and the dot blotting analysis:

Anti-T7-tag antibody was obtained from Novagen. Alkaliphosphatase-labeled anti-mouse IgG was purchased from Promega. PVDF membrane and cellulose membrane were from BIO-RAD and ADVANTEC.

2.2-2 Synthesis of fluorescent unnatural mutant streptavidin:

The process of synthesis and purification of fluorescent mutant streptavidin was shown in Fig.6. The wild type and mutant DNAs of streptavidin were synthesized by PCR, and then the mRNAs of wild type and mutant were synthesized by using of the products of PCR. Meanwhile, the tRNA-CA containing four-base anticondo from yeast was prepared like mRNAs, and then the unnatural amino acid aminoacyl-tRNA was synthesized by ligation of tRNA-CA and unnatural amino acid-pdCpA. The wild type and the mutant streptavidins were translated in *E.coli S30* extract, and then purified by His-tag purification and G-25 column.

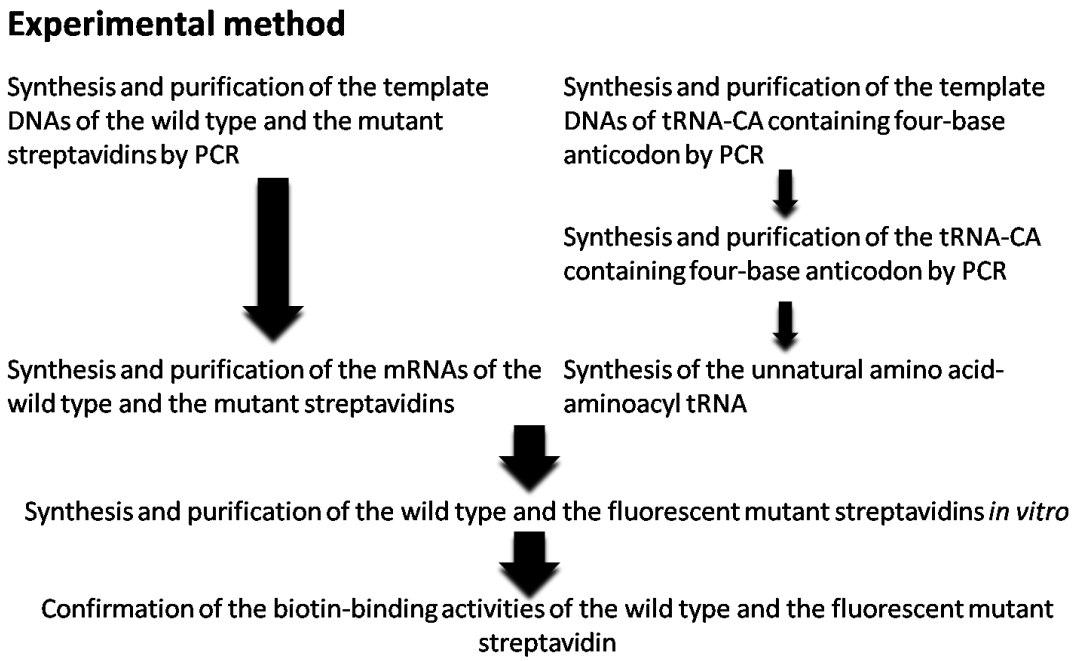

Fig.6 The process of preparation of fluorescent mutant streptavidins.

Synthesis and purification of the template DNAs of the wild type and the mutant streptavidins and tRNA-CA:

The materials were admixed for the RCP of the DNAs of wild type and mutant streptavidins as follows:

・ 10× Vent Buffer	5 µl
・ 2.5 mM dNTPs	4 µl
・ 20 µM primer T7up	2.5 µl
・ 20 µM primer T7term	2.5 µl
・ plasmid	0.5 µl
・ Vent DNA Polymerase	0.5 µl
・ milliQ	35 µl
Total	50 µl

The RCP of the DNAs of wild type and mutant streptavidins was operated as follows.

95℃ 5min – (95℃ 30sec, 55℃ 30sec, 72℃ 1min) × 25, 72℃ 7min,

and then purified by PCR purification kit (QIAquick®).

The products were confirmed by electrophoresis using 4% acrylamide/bisacrylamide PAGE.

The materials were admixed for the RCP of the tRNA-CA containing four-base anticodon as follows:

・ 10× Vent Buffer	5 µl
・ 2.5 mM dNTPs	4 µl
・ 20 µM primer M3	2.5 µl
・ 20 µM primer -CA	2.5 µl
・ plasmid	0.5 µl
・ Vent DNA Polymerase	0.5 µl
・ milliQ	35 µl
Total	50 µl

The RCP of the DNAs of wild type and mutant streptavidins was operated as follows.

95℃ 5min – (95℃ 30sec, 55℃30sec, 72℃ 1min) × 25, 72℃ 7min

and then purified by PCR purification kit (MinElute®).

The products were confirmed by electrophoresis using 6% acrylamide/bisacrylamide PAGE.

Synthesis and purification of the wild type and mutant streptavidins mRNAs and tRNA-CA:

The materials were admixed for the synthesis of the wild type and mutant streptavidins mRNAs as follows:

・10×T×buffer	5 μl
・25 mM NTPs	8 μl
・100 mM Spd	1 μl
・0.1% BSA	0.5 μl
・template DNA	10 μl
・RNasin	0.5 μl
・iPPase	0.5 μl
・T7 RNA Polymerase	2 μl
・milliQ	22.5 μl
Total	50 μl

The mixture was incubated at 37℃ for 6 hours.

The same amount of 5 M $AcONH_4$ was added into the reaction solution and cooled to 0℃ for 20 min. The supernatant fluid was removed after centrifugal separation (13000rpm, 4℃, 30 min). 200 μl of TE solution was added for dissolving the precipitates, and then TE solution was purified by 200 μl of phenol/chloroform mixture one time and 200 μl of chloroform one time. 10% amount of 3 M ACOK (pH4.5) as compared with TE solution and 3 times amount of ethanol as compared with TE solution was added, and then the supernatant fluid was removed after centrifugal separation (13000rpm, 4℃, 30 min) and dried. The concentration of mRNA was adjusted to 0.2 OD/μl by milliQ. The products were confirmed by electrophoresis by 4% acrylamide/bisacrylamide PAGE (Urea).

The materials were admixed for the synthesis of the tRNA-CA containing four-base anticodon as follows:

・ 10×T×buffer	5 µl
・ 25mM NTPs	8 µl
・ 100mM GMP	10 µl
・ 100mM Sqd	1 µl
・ 0.1% BSA	0.5 µl
・ DNA solution	20.5 µl
・ RNasin	0.5 µl
・ iPPase	0.5 µl
・ T7 RNA Polimerase	4 µl
Total	50 µl

The mixture was incubated at 37℃ for 12 hours.

The reaction solution was purified by ED52 column for separating the enzyme and DNAs. And then the tRNA-CA solution was purified by phenol/chloroform mixture one time and chloroform one time. 2.5 times amount of ethanol as compared with the tRNA-CA solution was added, and then the supernatant fluid was removed after centrifugal separation (13000rpm, 4℃, 30 min) and dried. The concentration of mRNA was adjusted to 0.1 OD/µl by milliQ. The products were confirmed by electrophoresis by 8% acrylamide/bisacrylamide PAGE (Urea).

Synthesis of the unnatural amino acid-aminoacyl tRNA:

Ordinarily, a -CCA polynucleotide sequence was appeared at the 3'terminal of the tRNAs. In this research, for synthesis of the unnatural amino acid-aminoacyl tRNA, the 3'terminal lacked CA polynucleotide of the tRNA containing four-base anticodon was used. On the other hand, an unnatural amino acid-aminoacyl pdCpA was synthesized. The unnatural amino acid aminoacyl-tRNA was synthesized by ligation of tRNA-CA and unnatural amino acid-pdCpA (Fig.7).

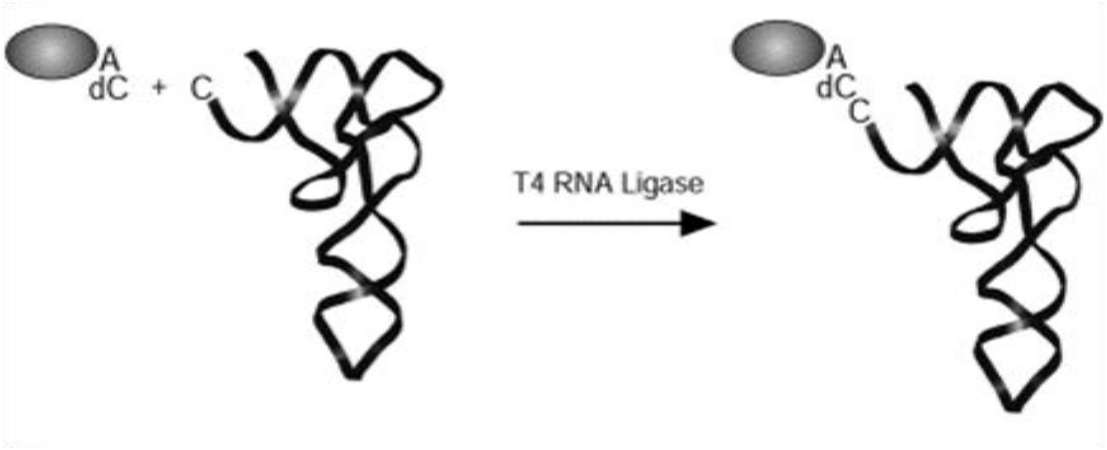

Fig.7 The unnatural amino acid-aminoacyl tRNA containing four-base codon was synthesized by ligation of tRNA-CA and unnatural amino acid-pdCpA.

The materials were admixed for the ligation of tRNA-CA and unnatural amino acid-pdCpA as follows:

・ 5×Ligation Buffer	4 µl
・ tRNA-CA sol	2.5 µl
・ non-natural amino acid-pdCpA/DMSO	2 µl
・ 0.1% BSA	0.4 µl
・ T4 RNA Ligase (25unit/mL)	1.2 µl
・ milliQ	9.9 µl
Total	20 µl

The mixture was incubated at 4°C for 2 hours.

2 times amount of 0.45 M ACOK (pH4.5) as compared with reaction solution and 9 times amount of ethanol as compared with reaction solution was added, and then the supernatant fluid was removed after centrifugal separation (13000rpm, 4℃, 30 min) and dried. The product was dissolved in 10% amount of 1 mM ACOK (pH4.5) as compared with reaction solution.

Translation of the wild type and mutant streptavidins:

The materials were admixed for the translation of the wild type streptavidins as follows:

・ LM+12	3 µl
・ mRNA (wild type)	2 µl
・ S30	2 µl
・ milliQ	3 µl
Total	10 µl

The materials were admixed for the translation of the mutant streptavidins as follows:

・ LM+12	3 µl
・ mRNA (mutant)	2 µl
・ unnatual amino acid-tRNA	1µl
・ S30	2 µl
・ milliQ	2 µl
Total	10 µl

The mixtures were incubated at 37℃ for 1 hour.

Confirmation of the synthesis of the wild type and the mutant streptavidins:

For identification of the protein synthesized by four-base method, T7-tag was added at the N terminus that allowed identifying the translated proteins by Western blot analysis in general. In this research, the synthesized mutant streptavidins were subjected to SDS-PAGE, and then blotted to the PVDF membrane. The bands of the wild type and the mutant streptavidins were confirmed by Western blotting analysis, in which the T7-tag of the N-terminal of the wild type and the mutant streptavidins were recognized with the anti-T7-tag antibody from mouse, and the secondary antibody for mouse antibody that was labeled with alkaliphosphatase.

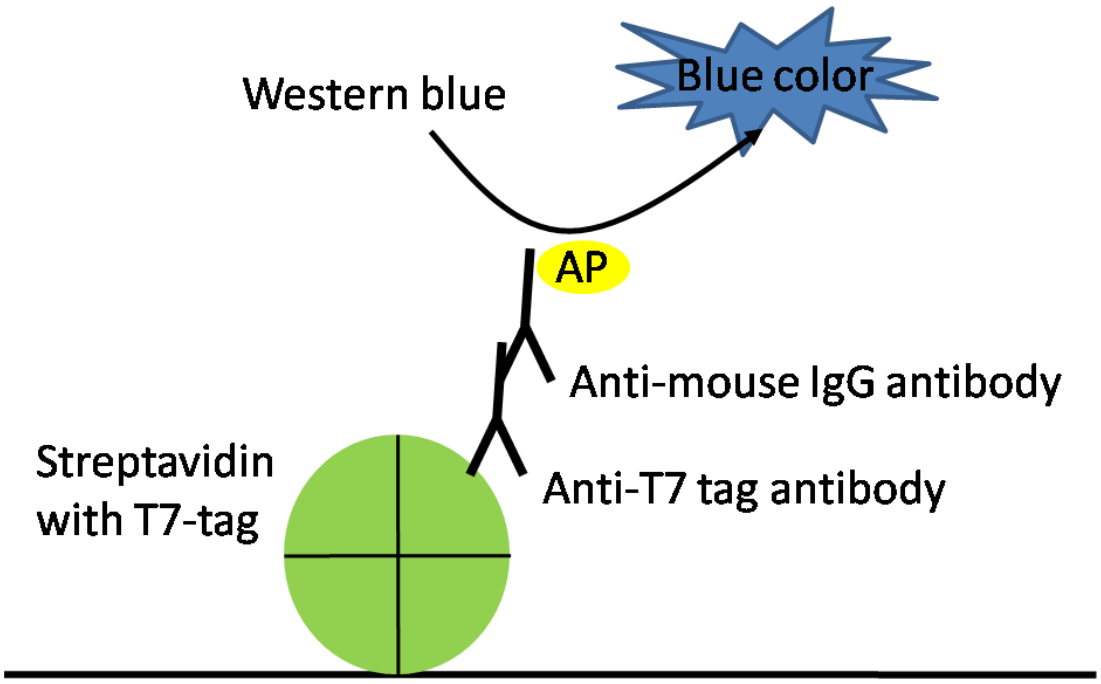

Fig.8 The Western blotting analysis of streptavidin.

Confirmation of the purification of the wild type and the mutant streptavidins:

More than six histadine amino acids at the end of a protein (either N or C terminus) are known as a 6X His-tag. Nickel is bound to an agarose bead by chelation using nitroloacetic acid (NTA) beads. The general method is to batch absorb the protein onto the column, by mixing the beads with the sample, then pouring the slurry of NTA beads and protein into a column, where low concentrations of phosphate and imidazole are used to remove low affinity bound proteins. If needed, the imdazole can be increased to 20 mM before most His tagged proteins are eluted. Finally, higher concentration of imidazole is used to elute the protein from the NTA-beads (Fig.9).

For purification of the protein synthesized by four-base method, His-tag was added at the C terminus that allowed purifying by the full-length of proteins His-tag purification system in general. For application of the fluorescent mutant streptavidins to the biotin molecular biosensor, the truncate peptides and the BFLAF-aminoacyl tRNAs that did not incorporated into the strepavidins must be eliminated completely. So the products were purified by His-tag purification and G-25 columns.

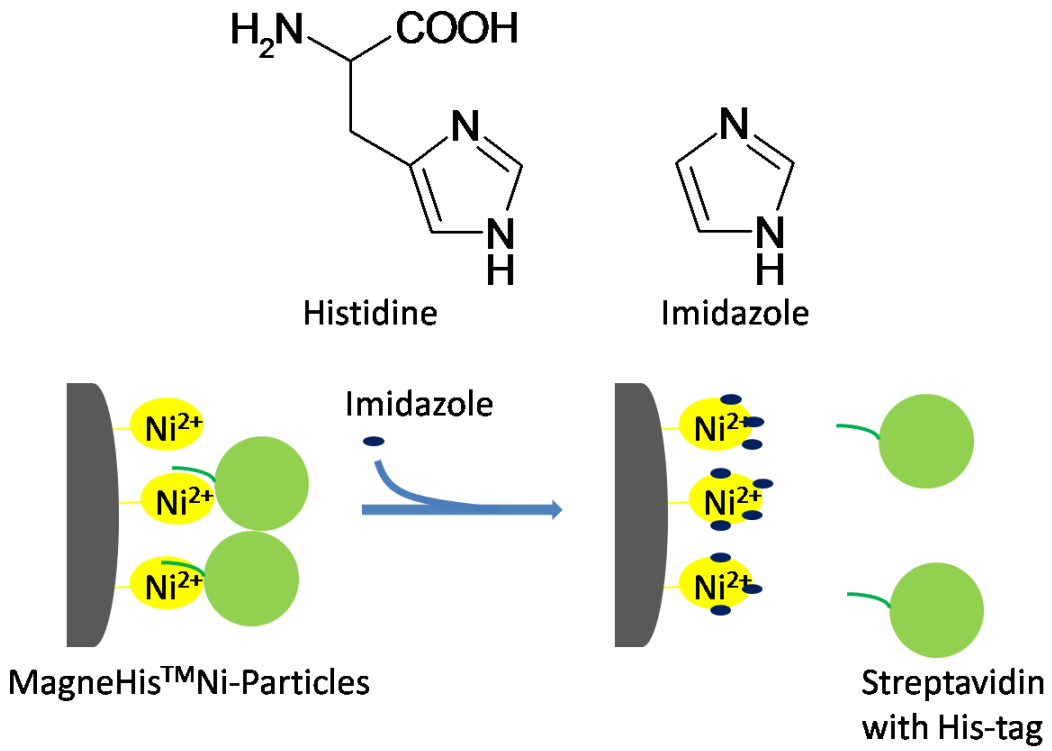

Fig.9 The His-tag purification of streptavidins.

Confirmation of the biotin-binding activity of the fluorescent mutant streptavidin:

A dot blot (or slot blot) is a technique in molecular biology used to detect biomolecules, and for detecting, analyzing, and identifying proteins. It represents a simplification of the northern blot, Southern blot, or western blot methods. In a dot blot the biomolecules to be detected are not first separated by electrophoresis. Instead, a mixture containing the molecule to be detected is applied directly on a membrane as a dot, and then is spotted through circular templates directly onto the membrane or paper substrate. This differs from the western blot because protein samples are not separated electrophoretically. This is then followed by detection by either nucleotide probes (for a northern blot and southern blot) or antibodies (for a western blot).

The technique offers significant savings in time, as chromatography or gel electrophoresis, and the complex blotting procedures for the gel are not required. However, it offers no information on the size of the target biomolecule. Furthermore, if two molecules of different sizes are detected, they will still appear as a single dot. Dot blots therefore can only confirm the presence or absence of a biomolecule or biomolecules which can be detected by the DNA probes or the antibody.

The biotin-binding activity of the wild type and mutant streptavidins was confirmed with dot blot analysis (Fig.10). 2 times amount of the mutant streptavidins as compared with wild type streptavidin were immobilized on the cellulose nitrate to bind with alkaline phosphatase-biotin, and then assayed with western blue for coloring. The coloring image of the dot on the blotting membrane was taken with a scanner and analyzed the spots density by the commercialized imaging software, the NIH ImageJ software.

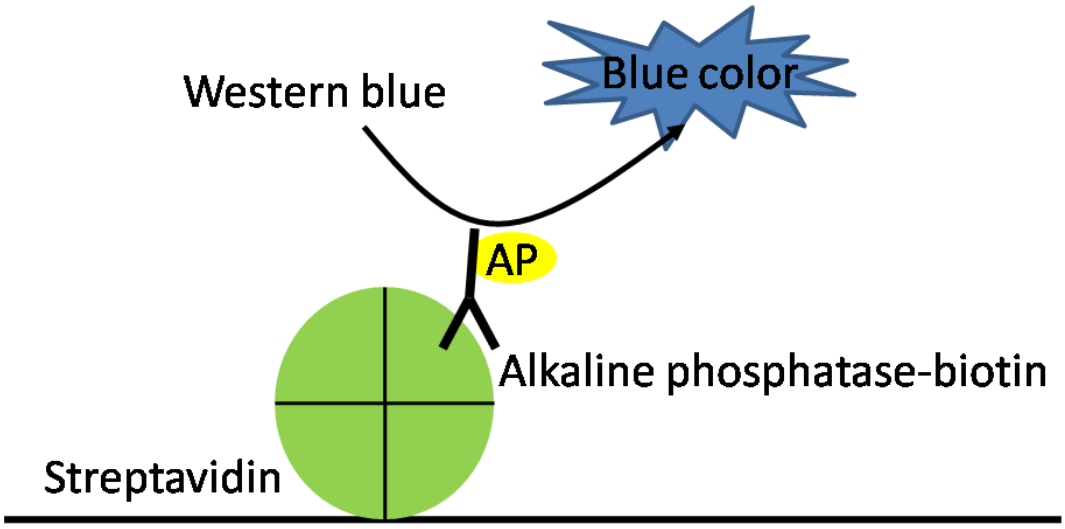

Fig.10 The dot blotting analysis of streptavidins.

2.2-3 Synthesis of the carbazole-labeled biotin:

Synthesis of 9-(2-aminetyl)-9H-carbazole hydrochloride:

The 0.9 M of borane-tetrahydrofuran solution (20 ml) was instilled into the 9-vinylcarbazole (5.8 g 0.03 mol) tetrahydrofuran solution under a stream of N_2 gas at room temperature. The mixture was stirred at room temperature for 2 hours. Thereafter, the trialkylborane solution was diluted with 10 ml of tetrahydrofuran and hydroxylamine-O-sulfonic acid (2.26 g, 20 mmol) was added, the reaction mixture was stirred at room temperature for 12 hours. The reaction mixture was then washed with 1 N of NaOH solution (100 ml) three times after diluted with diethyl ether (20 ml). The organic phase that was dried by $MgSO_4$ was reacted with ethereal HCl (1 M, 10 ml) to precipitate the amine as 9-(2-aminetyl)-9H-carbazole hydrochloride. The solid was washed with diethyl ether and dried to yield 0.83 g (14%) [20].

Synthesis of quencher-labeled biotin:

The 10 mM of 9-(2-aminetyl)-9H-carbazole hydrochloride in methanol (5 ml) was added into 10 mM of N-Succinimidyl D-Biotin or EZ-Link® NHS-LC-Biotin or EZ-Link® NHS-LC-LC-Biotin that dissolved in Tris-HCl buffer pH8.3 (5 ml) were stirred at 0 ℃ for 3 hours. The solid was washed with diethyl ether, water and evaporated to dryness, yielded carbazole-labeled biotin carbazole-LC-biotin and carbazole-LC-LC-biotin all more than 95% [21].

2.2-4 Experimental procedure for fluorescence biosensing:

The carbazole-labeled biotin was prepared with DMSO. The samples contained 10 µl of solution of fluorescent mutant streptavidin, 10 µl of solution of carbazole-labeled biotin, 10µl of solution of natural biotin, and diluted to 100 µl with HKM buffer（100 mM KCl, 25 mM Hepes, 5 mM $MgCl_2$, pH adjusted to 7.4 with KOH). A fluorescence spectrometer (JASCO FP-6500) was used to measure excitation and emission spectra of the sample solutions with the slit width in 5 nm for both excitation and emission.

2.3 Result and discussion:

2.3-1 Confirmation of the synthesis of the unnatural mutant streptavidins:

Preparation of fluorescent mutant streptavidin:

Confirmation of the results of PCR:

Confirmation of the results of the DNAs of wild type and mutant streptavidins synthesized by PCR:

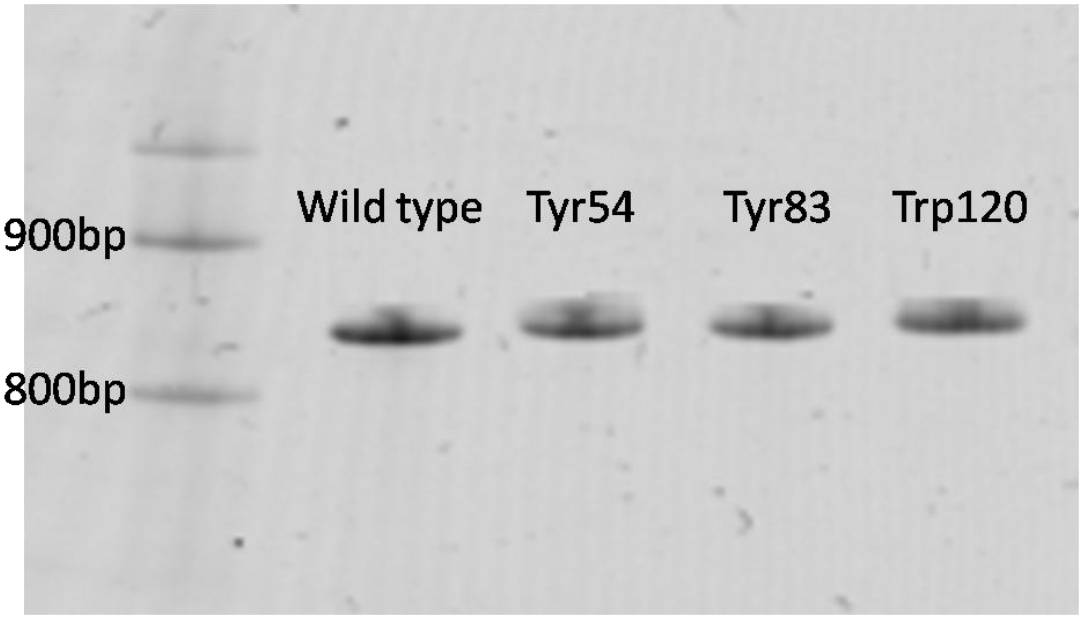

Fig.11 The bands of purified template DNAs of wild type and mutant streptavidins were observed between 800bp~900bp. This result demonstrated that the template DNAs of wild type and mutant streptavidins were synthesized successfully.

The products of PCR were subjected to 4% acrylamide/bisacrylamide PAGE to compare the molecular weight. The bands of the template DNAs of wild type and mutant streptavidins were observed at the almost same molecular weight between 800bp to 900bp (Fig.11). This result demonstrated that the template DNAs of wild type and mutant streptavidins were synthesized successfully by PCR.

Confirmation of the results of the DNAs of tRNA-CA containing four-base anticodon synthesized by PCR:

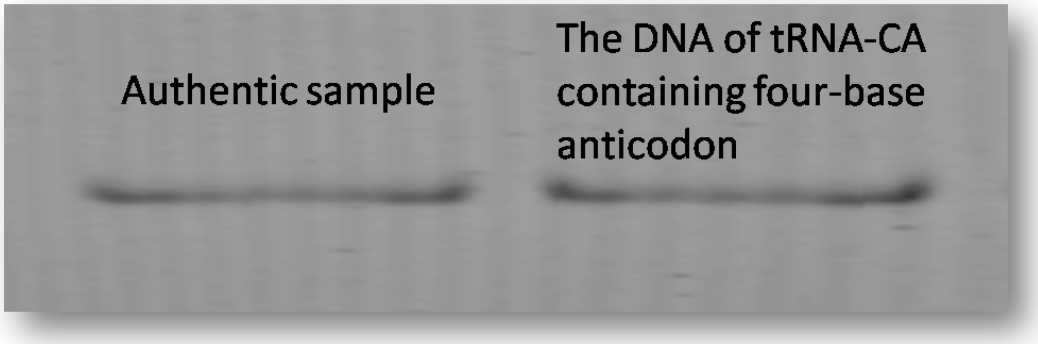

Fig.12 The band of the DNAs of tRNA-CA containing four-base anticodon was observed at the same position of authentic sample. This result demonstrated that the DNA of tRNA-CA containing four-base anticodon was synthesized successfully.

The products of PCR were subjected to 6% acrylamide/bisacrylamide PAGE to compare the molecular weight. The stock solution was used as an authentic sample for the confirmation of the result of PCR. The band of the template DNA of tRNA-CA containing four-base anticodon was observed at the almost same molecular weight with the authentic sample (Fig.12). This result demonstrated that the template DNAs of tRNA-CA containing four-base anticodon was synthesized successfully by PCR.

Confirmation of the results of synthesis of the RNAs:

Confirmation of the results of synthesis of the RNAs of the wild type and mutant streptavidins:

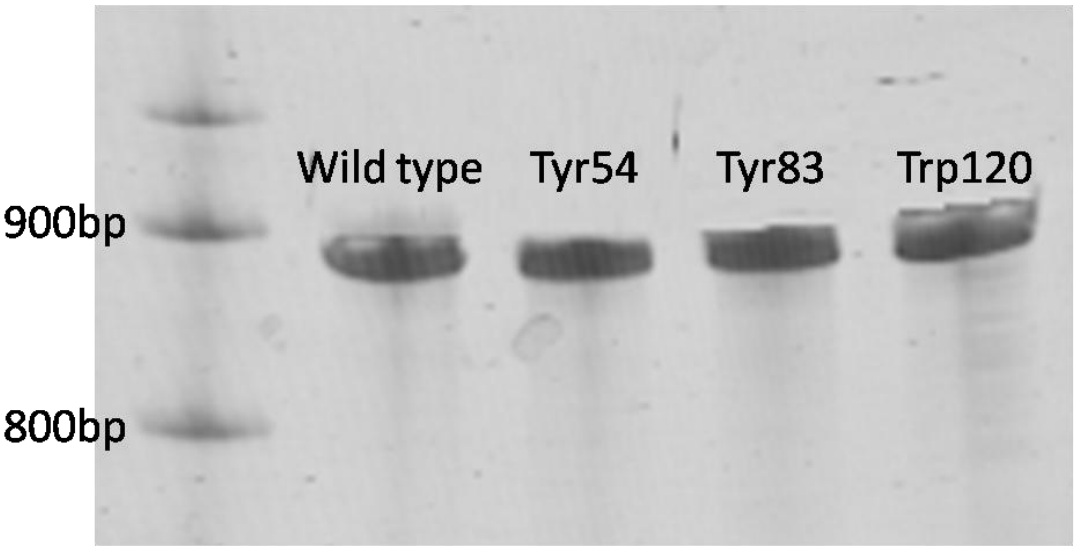

Fig.13 The bands of purified mRNAs of wild type and mutant streptavidins were observed between 800bp~900bp. This result demonstrated that the mRNAs of wild type and mutant streptavidins were synthesized successfully.

The RNAs of the wild type and mutant streptavidins were synthesized and purified from the template DNAs. The products were diluted to the 10% as compared with stock solution and subjected to 4% acrylamide/bisacrylamide PAGE (Urea) to compare the molecular weight. The bands of the RNAs of wild type and mutant streptavidins were observed at the almost same molecular weight between 800bp to 900bp (Fig.13). This result demonstrated that the RNAs of wild type and mutant streptavidins were synthesized successfully from the template DNAs.

Confirmation of the results of synthesis of the tRNA-CA containing four-base anticodon:

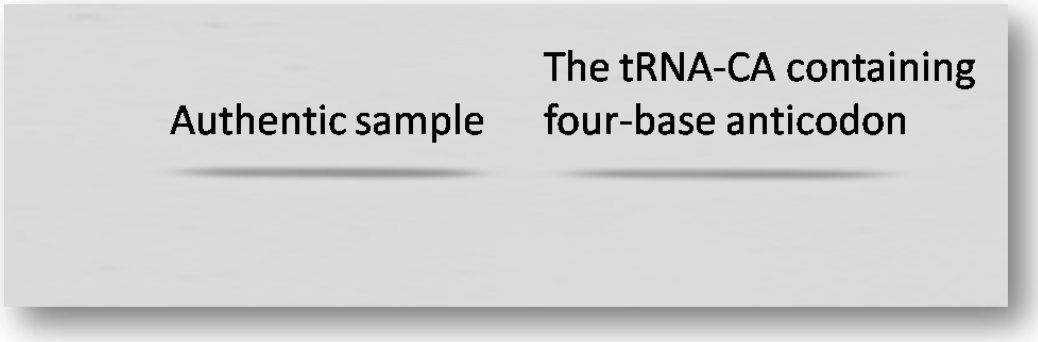

Fig.14 The band of the tRNA-CA containing four-base anticodon was observed at the same position of authentic sample. This result demonstrated that the tRNA-CA containing four-base anticodon was synthesized successfully.

The tRNA-CA containing four-base anticodon was synthesized and purified from the template DNAs. The products were diluted to the 10% as compared with stock solution and subjected to 8% acrylamide/bisacrylamide PAGE (Urea) to compare the molecular weight. The band of the tRNA-CA containing four-base anticodon was observed at the almost same molecular weight with the authentic sample from laboratory of Prof. Hohsaka of Japan advanced institute of science and technology (JAIST). (Fig.14). This result demonstrated that the RNAs of wild type and mutant streptavidins were synthesized successfully from the template DNAs.

Confirmation of the translation of the wild type and mutant streptavidins:

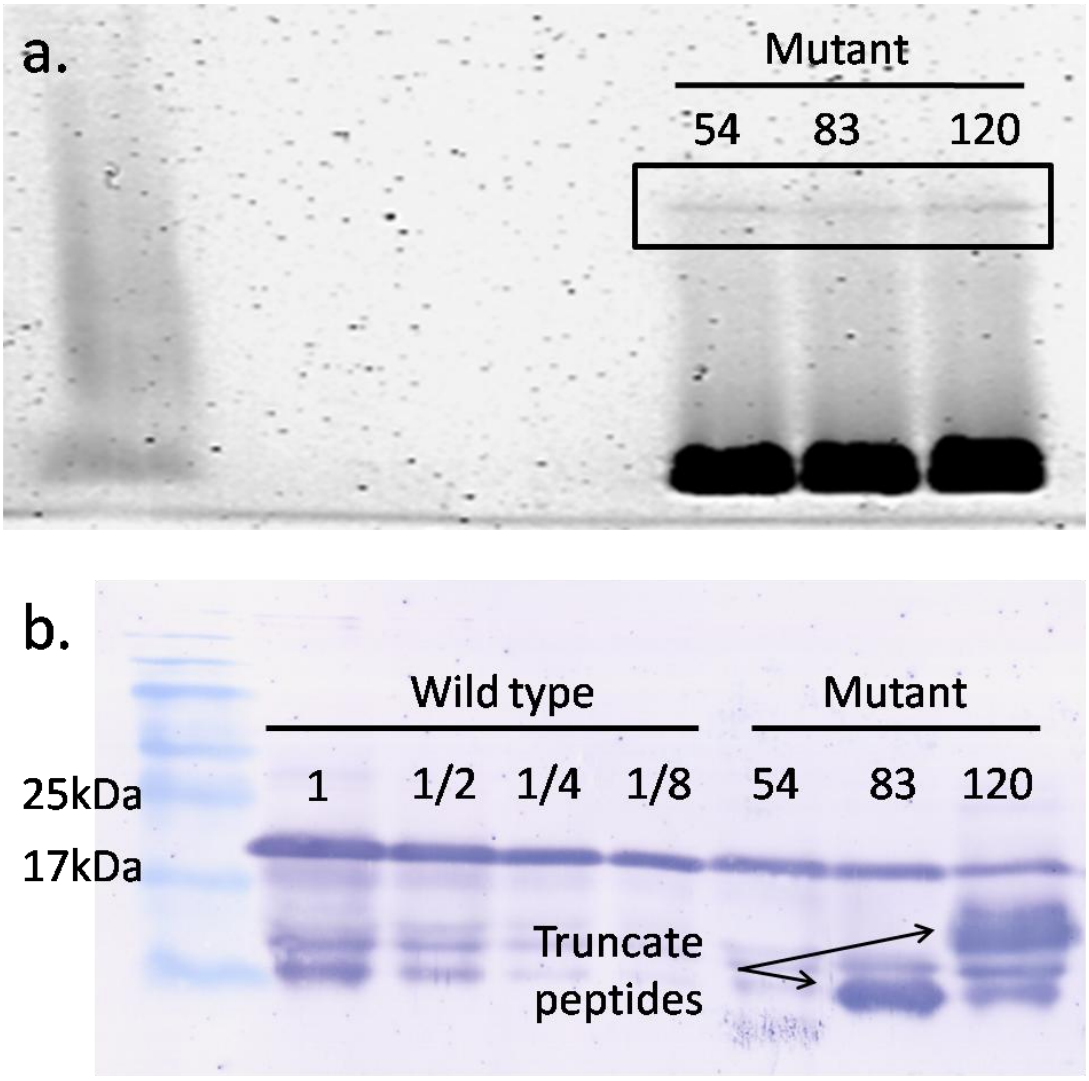

Fig.15 (a) The result of fluorescence imaging analysis. Three bands of Tyr54BFLAF, Tyr83BFLAF and Trp120BFLAF of fluorescent mutant streptavidin were draw with the black box.
(b) The result of Western blotting. BFLAF was incorporated into streptavidin by using a CGGG four-base codon. The bands of wild type and mutant streptavidins were observed around 20 kDa.

The wild type, Tyr54BFLAF, Tyr83BFLAF and Trp120BFLAF mutant streptavidins were translated by *in vitro* translation. 1.5 times amount of the fluorescent mutant streptavidins solution as compared with wild type streptavidin was subjected to SDS-PAGE to compare the molecular weight. The bands of three fluorescent mutant streptavidin would be confirmed by fluorescence imaging analysis that excited with 488nm and observed at 530nm because of BFLAF (λexmax=505 nm, λemmax=514 nm)(Fig.15a). On the other hand, the bands of three mutant streptavidins were confirmed by Western blotting, in which the T7-tag of the N-terminal of the mutant streptavidin was recognized by anti-T7-tag antibody from mouse, and an antibody for mouse was used as a secondary antibody that was labeled with alkaliphosphatase. The full-length of streptavidin (20 kDa) was obtained only in the presence of BFLAF into the translation system (Fig.14b). The results of fluorescence imaging analysis and Western blotting indicated that the BFLAF were incorporated into streptavidin at each specific position to make the full-length of streptavidin. The bands of the wild type and three mutant streptavidin in blotting membrane were seen at the almost same molecular weight of 20 kDa. The incorporation efficiency of the BFLAF, however, strongly depends on the structure of its side chain and the incorporated site. The relative yield of the full-length streptavidin obtained in the presence of the BFLAF aminoacyl-tRNA was determined by comparing the band density of the full-length product with those of serially diluted wild type streptavidin. The protein yields of Tyr54BFLAF, Tyr83BFLAF and Trp120BFLAF mutant streptavidin were analyzed to 8.2%, 7.9% and 7.8%, respectively as compared with the band density of wild type streptavidin as 100% with NIH ImageJ software.

At the below of the bands of Tyr83BFLAF and Trp120BFLAF mutant streptavidin in the result of Western blotting analysis, the bands of truncate peptides were also observed, and also at the bottom of the result of fluorescence imaging analysis, the BFLAF-aminoacyl tRNAs that did not incorporated into the strepavidins were also observed.

For application of the fluorescent mutant streptavidins to the biotin molecular biosensor, the truncate peptides and the BFLAF-aminoacyl tRNAs that did not incorporated into the strepavidins must be eliminated completely. So the products were purified by His-tag purification and G-25 columns.

Confirmation of the purification of the wild type and mutant streptavidins:

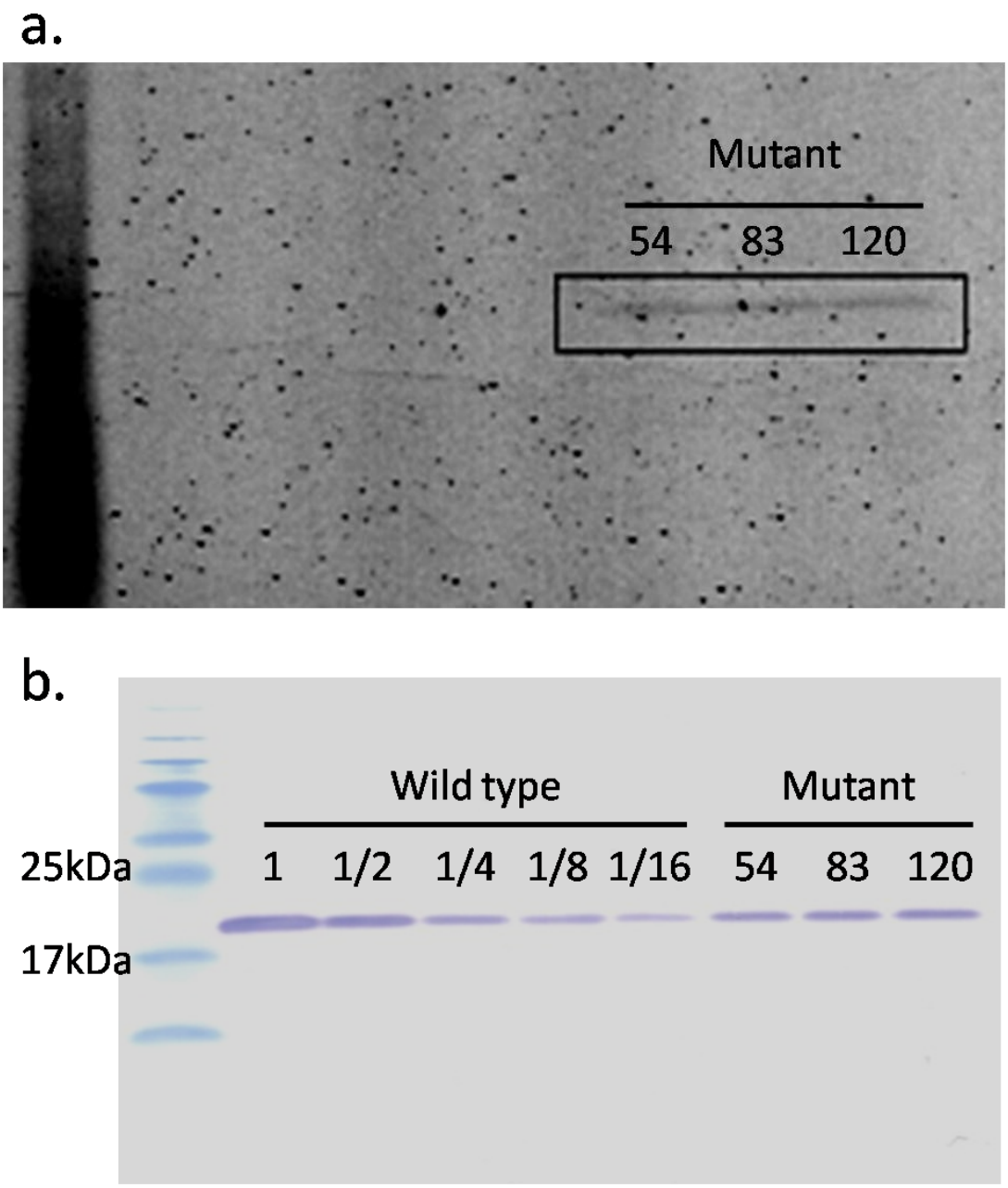

Fig.16 (a) The result of fluorescence imaging analysis. Three bands of Tyr54BFLAF, Tyr83BFLAF and Trp120BFLAF of fluorescent mutant streptavidin were draw with the black box.
(b) The result of Western blotting. BFLAF was incorporated into streptavidin by using a CGGG four-base codon. The bands of wild type and mutant streptavidins were observed around 20 kDa.

The wild type, Tyr54BFLAF, Tyr83BFLAF and Trp120BFLAF mutant streptavidins were purified by His-tag purification and G-25 columns. 3 times amount of the fluorescent mutant streptavidins solution as compared with wild type streptavidin was subjected to SDS-PAGE to compare the molecular weight. The bands of three fluorescent mutant streptavidin would be confirmed by fluorescence imaging analysis that excited with 488nm and observed at 530nm (Fig.16a). On the other hand, the bands of three mutant streptavidins were confirmed by Western blotting, the full-length of streptavidin (20 kDa) was obtained only in the presence of BFLAF into the translation system (Fig.16b). The results of fluorescence imaging analysis and Western blotting indicated that the BFLAF were incorporated into streptavidin at each specific position to make the full-length of streptavidin. The bands of the wild type and three mutant streptavidin in blotting membrane were seen at the almost same molecular weight of 20 kDa. The incorporation efficiency of the BFLAF, however, strongly depends on the structure of its side chain and the incorporated site. The relative yield of the full-length streptavidin obtained in the presence of the BFLAF aminoacyl-tRNA was determined by comparing the band density of the full-length product with those of serially diluted wild type streptavidin. The protein yields of Tyr54BFLAF, Tyr83BFLAF and Trp120BFLAF mutant streptavidin were analyzed to 7.4%, 7.9% and 8.2%, respectively as compared with the band density of wild type streptavidin as 100% with NIH ImageJ software.

2.3-2 Confirmation of the biotin binding activity of the unnatural mutant streptavidins:

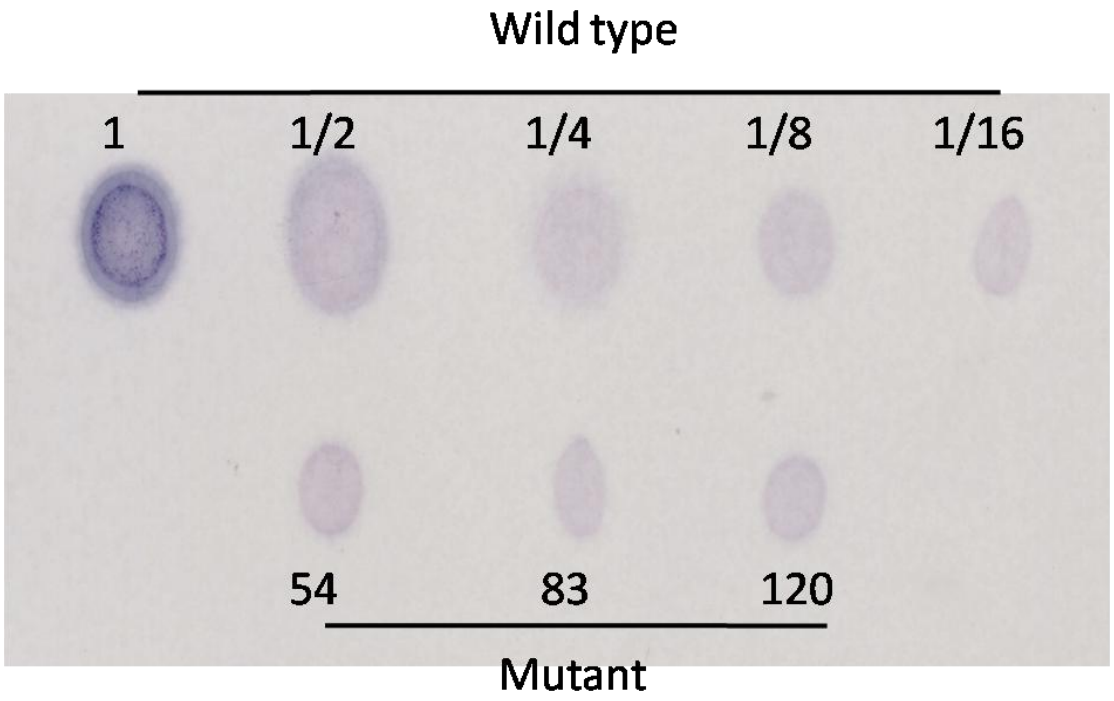

Fig.17 The result of dot blotting. The biotin binding activities of these fluorescent mutant streptavidins were evaluated by a dot blot analysis using an Alkaline Phosphatase-biotin.

The biotin binding activities of the wild type and the mutant streptavidins were evaluated by dot blotting using alkaline phosphatase-biotin. For confirmation of the biotin binding activities of the mutant streptavidins accurately and easily, 2 times amount of each mutant streptavidin solution as compared with wild type streptavidin solution was blotted on the membrane. Therefore, the protein amounts of Tyr54BFLAF, Tyr83BFLAF and Trp120BFLAF mutant streptavidins blotted on the membrane were 14.8%, 15.8% and 16.4% of that of wild type streptavidin from Western blotting analysis. The blot density of Tyr54BFLAF, Tyr83BFLAF and Trp120BFLAF were 9.6%, 9.6% and 9.7%, respectively as compared with the wild type streptavidin with NIH ImageJ software. Therefore, the biotin-affinity of Tyr54BFLAF, Tyr83BFLAF and Trp120BFLAF mutant streptavidins was evaluated to 65%, 61% and 59%, respectively as compared with the wild type streptavidin. The results indicated that the mutant streptavidin containing BFLAF at positions Tyr83 and Trp120 retained as strong biotin binding activity as wild type streptavidin (Fig.17). These positions locate at surface regions of the beta-barrel structure or at an interface region of a biotin binding pocket that may be influential in biotin binding activities little.

2.3-3 Fluorescence analysis of the fluorescent unnatural mutant streptavdins:

The excitation spectra and fluorescent spectra of Tyr54BFLAF, Tyr83BFLAF and Trp120BFLAF fluorescent mutant streptavidins were shown in Fig.17. The excitation spectra of the Tyr54BFLAF, Tyr83BFLAF and Trp120BFLAF fluorescent mutant streptavidins were observed at 530 nm, the fluorescent spectra of the Tyr54BFLAF, Tyr83BFLAF and Trp120BFLAF fluorescent mutant streptavidins were excited at 480 nm. The maximum excitation wavelengths of the Tyr54BFLAF, Tyr83BFLAF and Trp120BFLAF fluorescent mutant streptavidins were observed at 505 nm, and and the maximum fluorescent wavelengths of the Tyr54BFLAF, Tyr83BFLAF and Trp120BFLAF fluorescent mutant streptavidins were observed at 510 nm. A fluorescence spectrometer (JASCO FP-6500) was used to measure excitation and emission spectra of the sample solutions with the slit width in 3 nm for both excitation and emission.

Excitation spectrum and fluorescence spectrum of Tyr54BFLAF fluorescent mutant streptavidins:

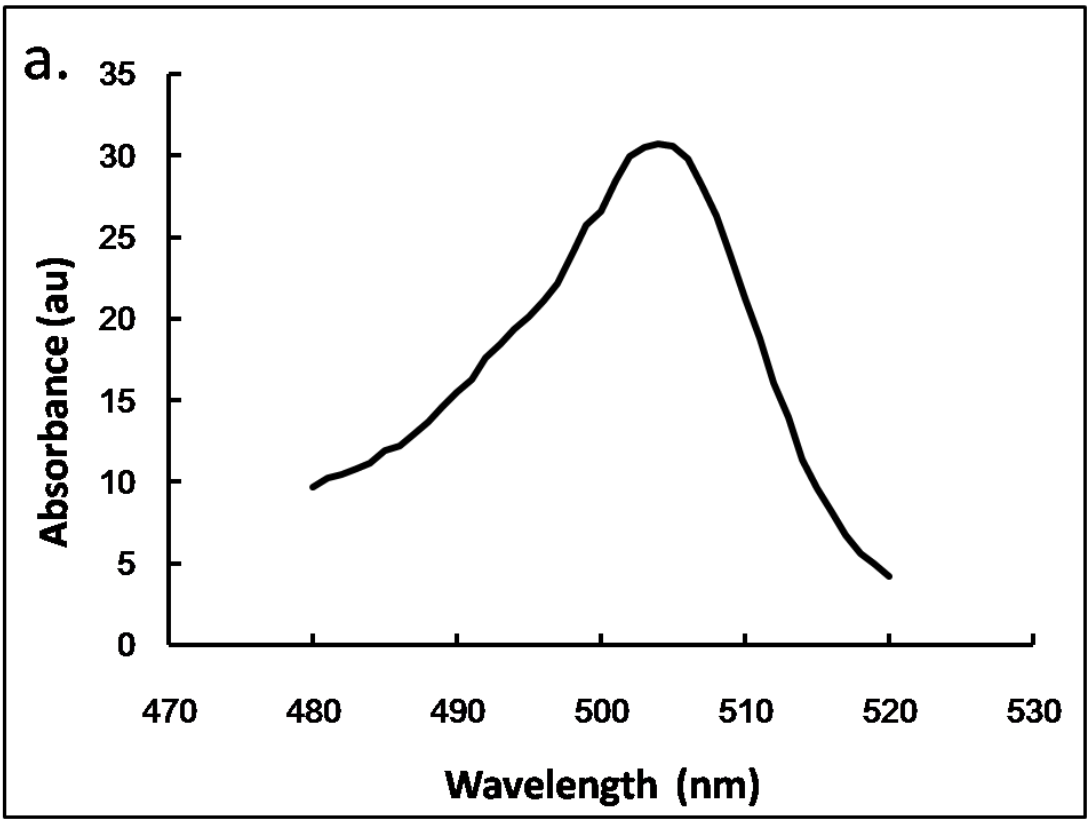

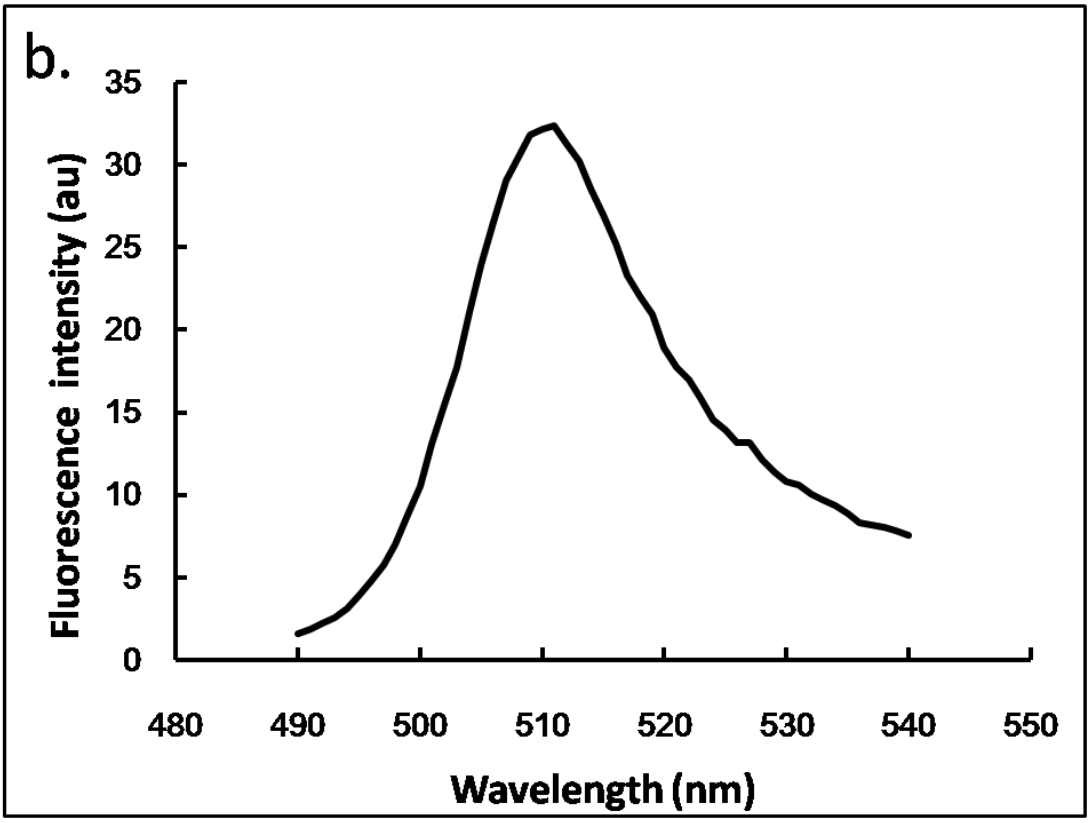

Excitation spectrum and fluorescence spectrum of Tyr83BFLAF fluorescent mutant streptavidins:

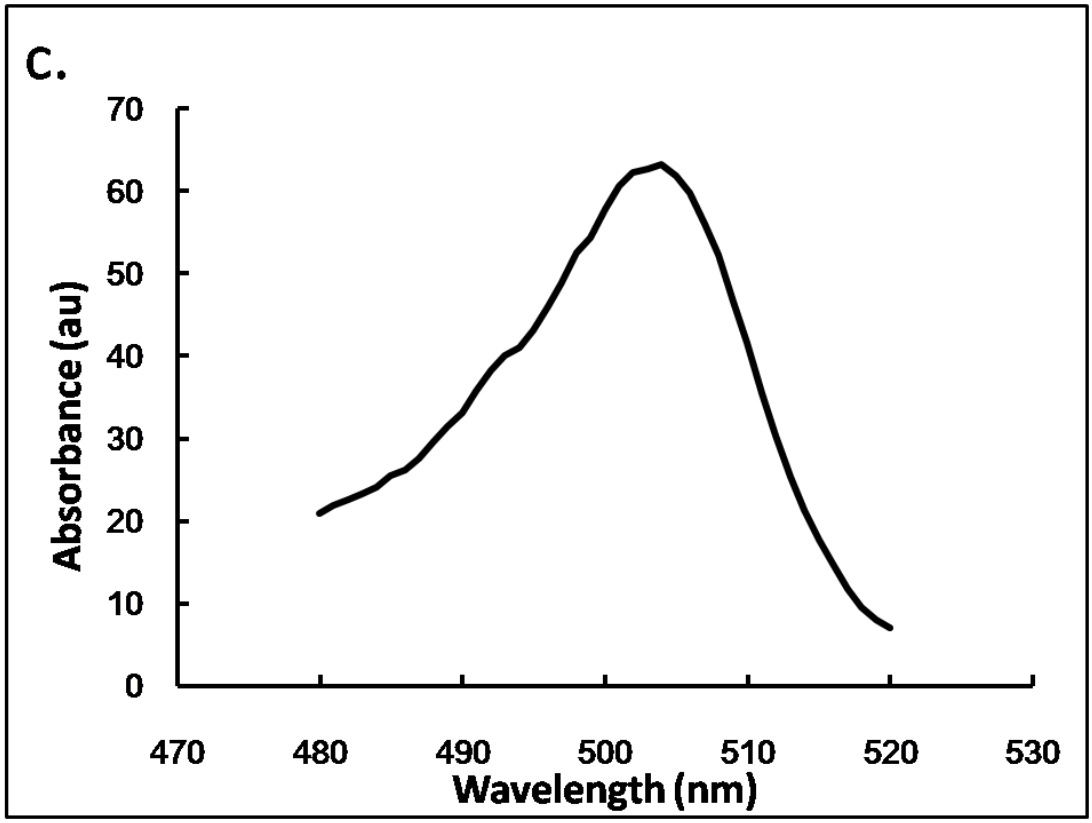

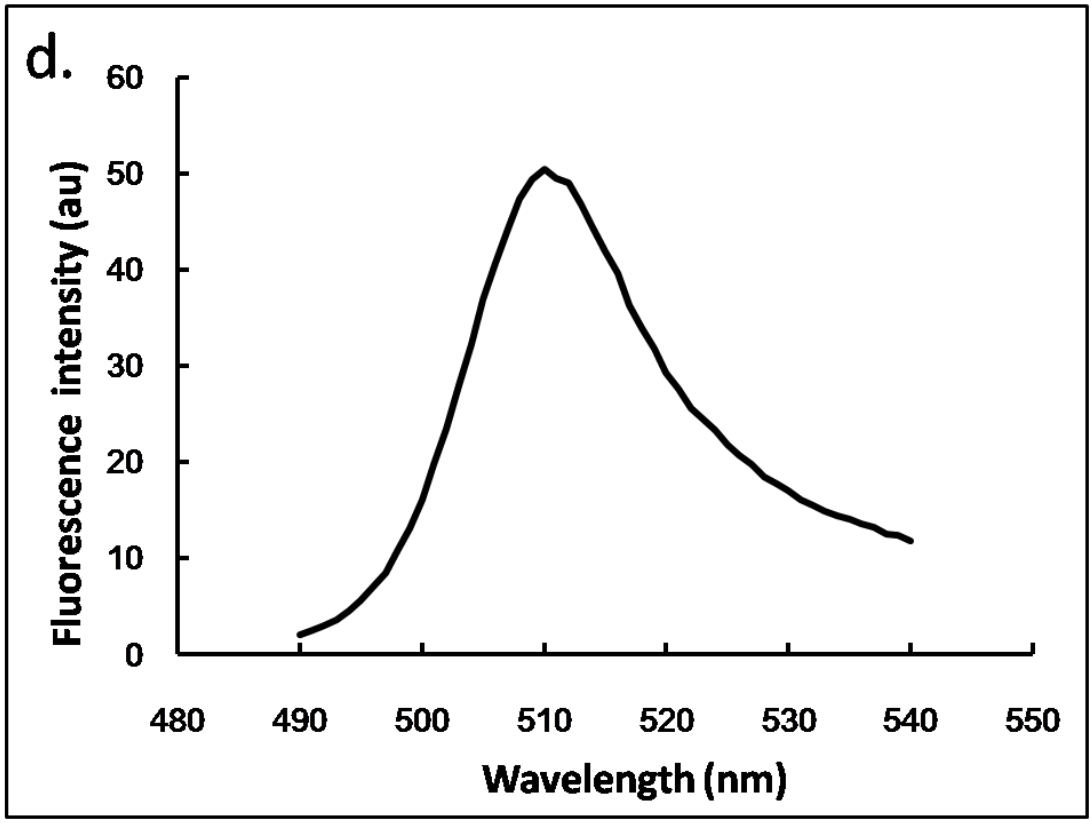

Excitation spectrum and fluorescence spectrum of Trp120BFLAF fluorescent mutant streptavidins:

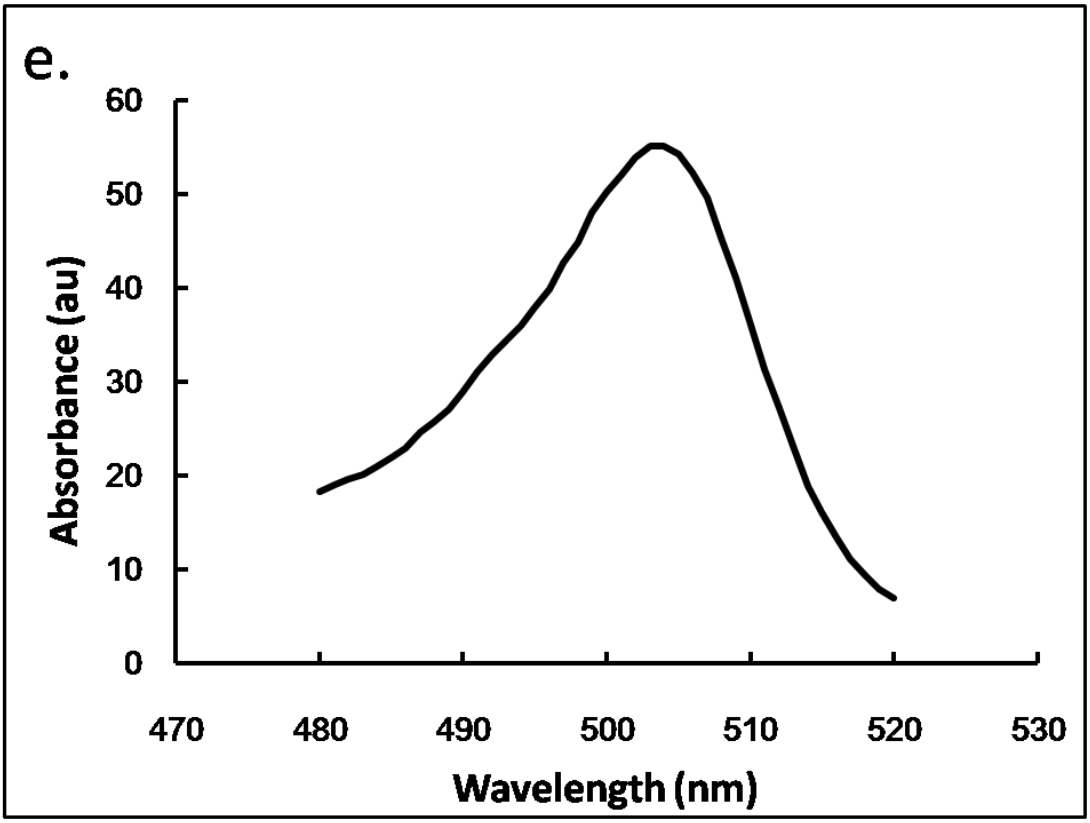

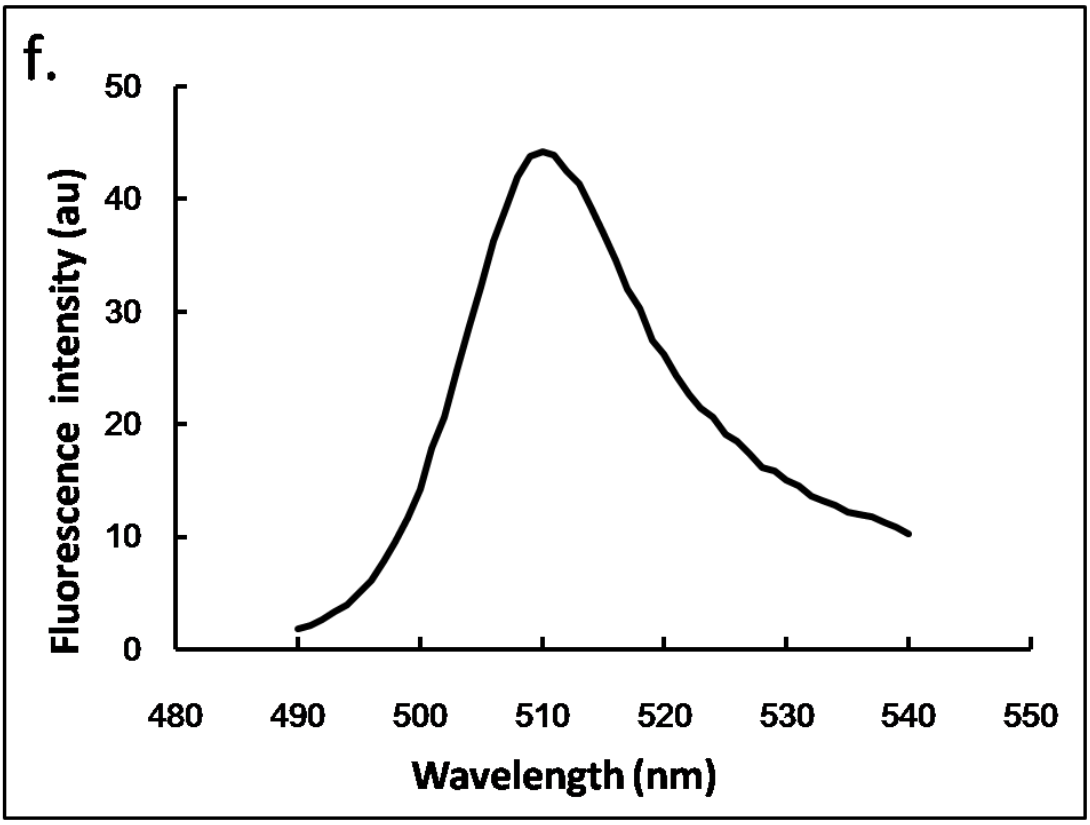

Fig.18 (a) (c) (e) The excitation spectra of Tyr54BFLAF, Tyr83BFLAF and Trp120BFLAF fluorescent mutant streptavidins. The excitation spectra were observed at 530 nm, and the maximum excitation wavelengths were observed at 505 nm.
(b) (d) (f) The fluorescent spectra of Tyr54BFLAF, Tyr83BFLAF and Trp120BFLAF fluorescent mutant streptavidins. The fluorescent spectra were excited at 480 nm, and the maximum fluorescent wavelengths were observed at 510 nm.

2.3-4 Fluorescence measure of the unnatural mutant streptavidins upon binding of carbazole-labeled biotin and free biotin:

Fluorescence quenching of fluorescent mutant streptavidin upon addition with carbazole-labeled biotin:

Before the experiment of fluorescence quenching of fluorescent mutant streptavidin upon addition with carbazole biotin, 100 nM of natural biotin was added into the solution of fluorescent mutant streptavidin for confirming the effect of the natural biotin. Actually, the effect of fluorescence intensity from natural biotin was little (Fig.19a, b, c).

The Fluorescence spectra of fluorescent mutant streptavidin of Tyr54BFLAF, Tyr83BFLAF and Trp120BFLAF upon addition with carbazole-labeled biotin were measured. There was hardly any change of the fluorescence intensity of Tyr54BFLAF and Tyr83BFLAF presence (100 nM) and absence of carbazole-labeled biotin. Tyr54 and Tyr83, BFLAF incorporated into these positions are escaping from carbazole-labeled biotin. The energy transfer between BFLAF incorporated into the position of Tyr54 or Tyr83 of streptavidin to carbazole-labeled biotin would be difficult to occur (Fig.19a, b).

By contrast, Trp120BFLAF of fluorescent mutant streptavidin, a marked quenching was occurred upon addition with carbazole-labeled biotin (100 nM). The fluorescence intensity of the Trp120BFLAF is 1.4 time that of Trp120BFLAF in the absence of carbazole-labeled biotin (100 nM) (Fig3.c). Furthermore, concentration dependence that quenching of Trp120BFLAF upon addition with carbazole-labeled biotin was observed (Fig.19c).

Quenching of Trp120BFLAF was observed from addition with 10 nM of carbazole-labeled biotin. However, BFLAF, were strongly depends on the structure of its side chain, incorporated into streptavidin, would induce weakening of biotin-affinity of Trp120BFLAF. Whereupon, carbazole-labeled biotin, it would be difficult to binding to the streptavidin than natural biotin because of the structure of its side chain (Fig.19c).

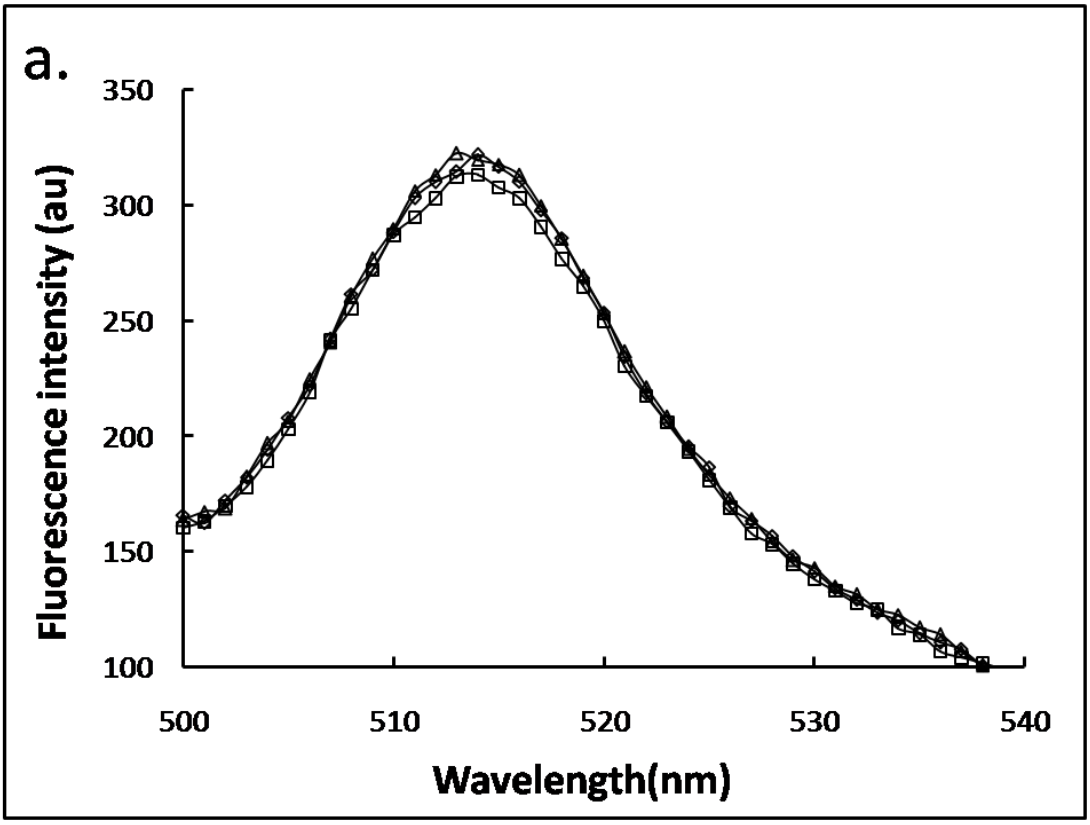
a.
Fluorescence intensity (au)
350
300
250
200
150
100
500
510
520
530
540
Wavelength(nm)

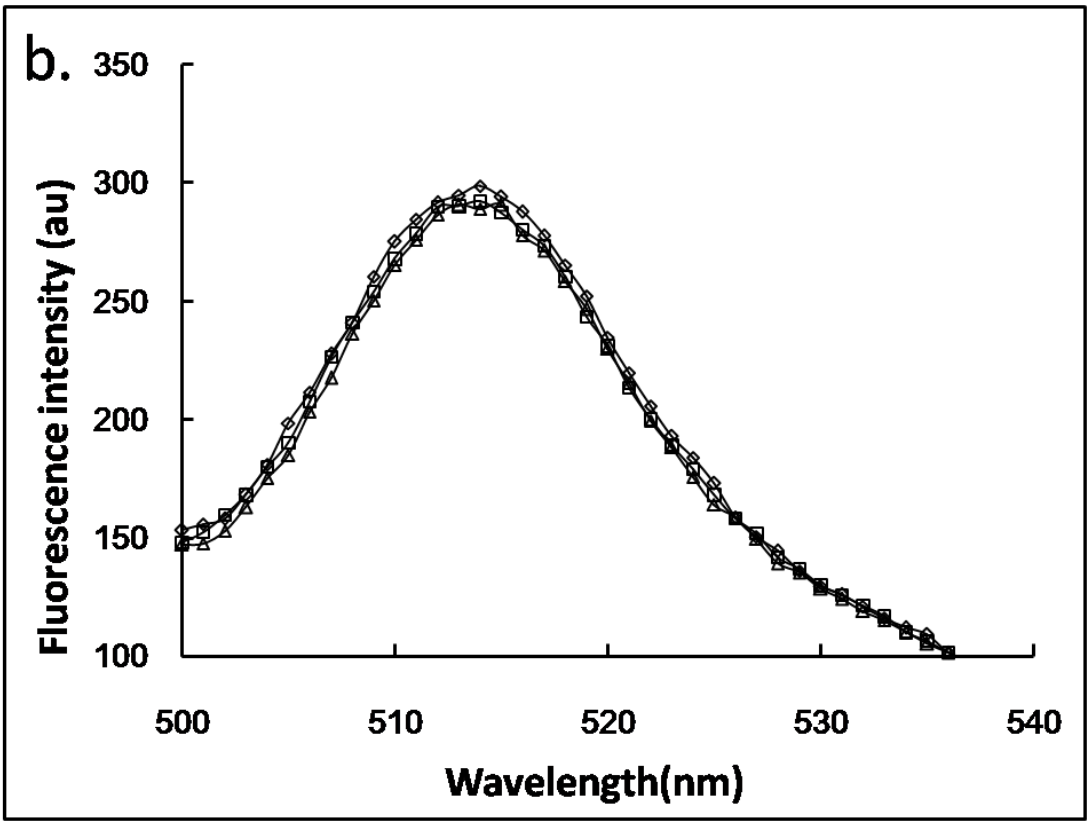
b.
Fluorescence intensity (au)
350
300
250
200
150
100
500
510
520
530
540
Wavelength(nm)

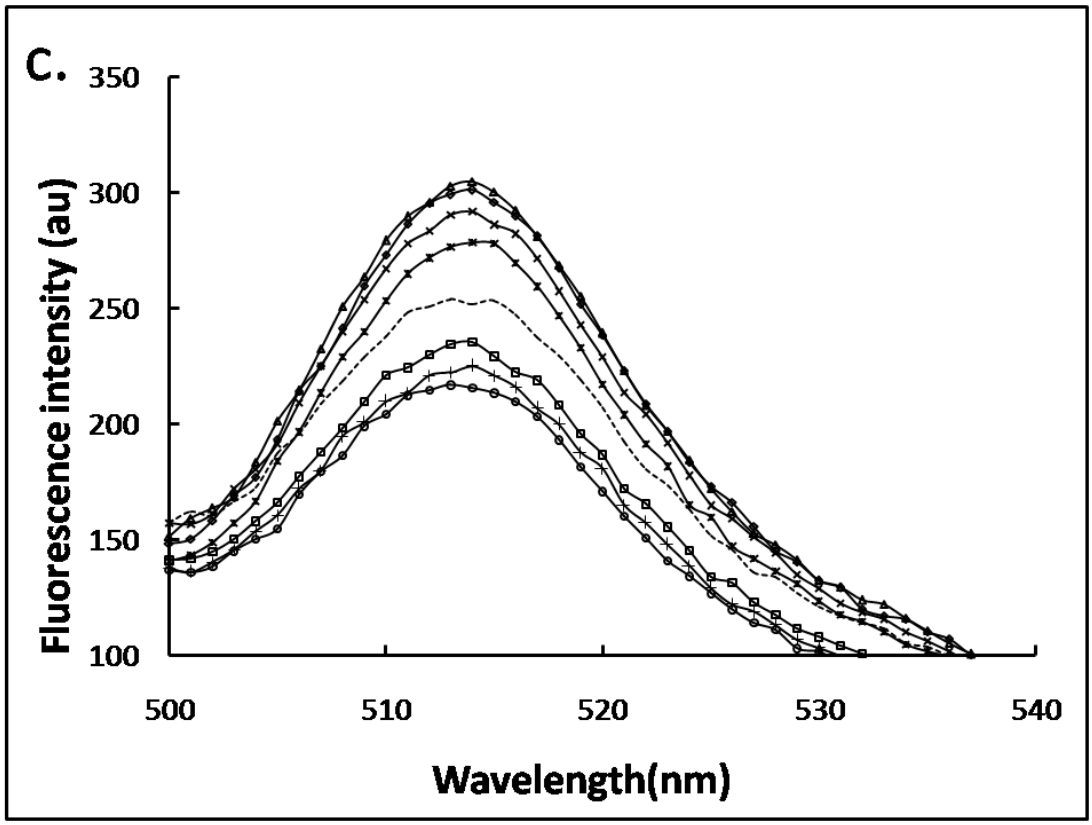
c.
Fluorescence intensity (au)
350
300
250
200
150
100
500
510
520
530
540
Wavelength(nm)

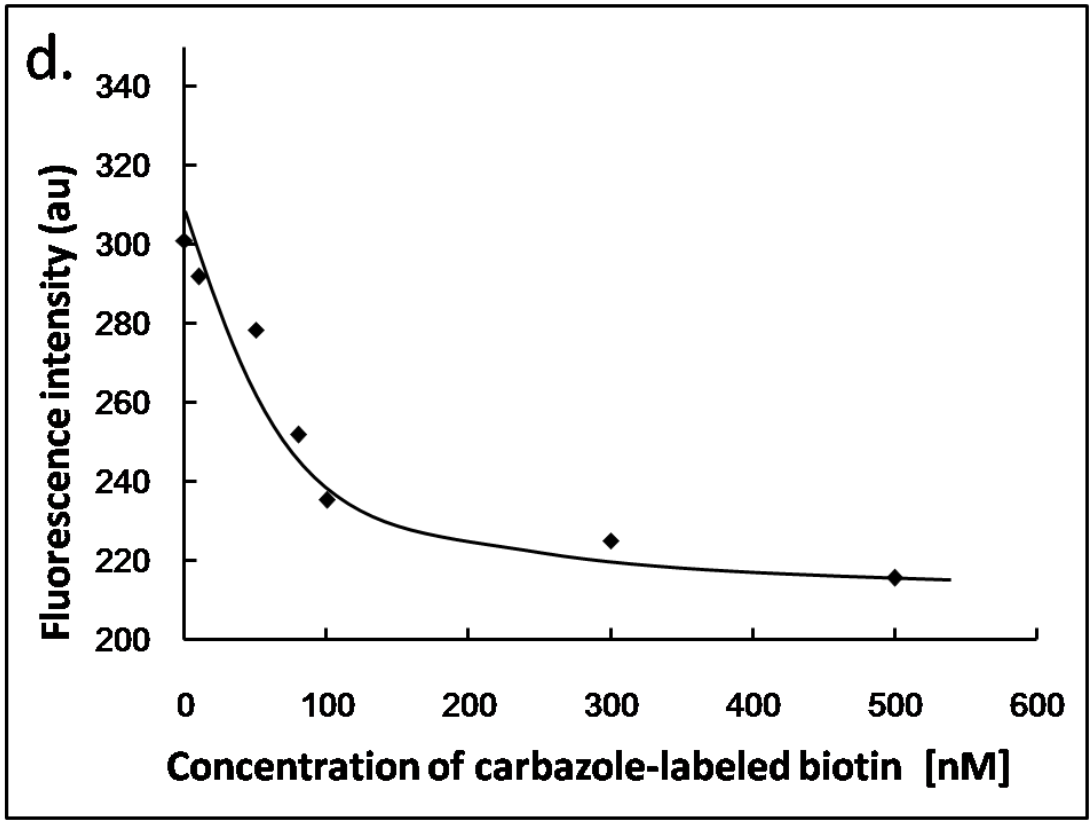
d.
Fluorescence intensity (au)
340
320
300
280
260
240
220
200
0
100
200
300
400
500
600
Concentration of carbazole-labeled biotin [nM]

Fig.19 (a) (b) Fluorescence spectra of the Tyr54BFLAF and the Tyr83BFLAF mutant streptavidin only (—◇—); Fluorescence spectra of the Tyr54BFLAF and the Tyr83BFLAF mutant streptavidin in the presence of 100 nM of natural biotin (—△—) or 100 nM of carbazole-labeled biotin (—□—); There was no change in the fluorescence intensity upon addition of natural biotin or carbazole-labeled biotin for the Tyr54BFLAF and the Tyr83BFLAF mutant streptavidin.

(c) Fluorescence spectra of the Trp120BFLAF mutant streptavidin only (—◇—), in the presence of 100 nM of natural biotin (—△—), or 10 nM (—✕—), or 50 nM (—■—), or 80 nM (·····), or 100 nM (—□—), or 300 nM (—┼—), or 500 nM (—○—) of carbazole-labeled biotin. Marked fluorescence quenching was observed for the Trp120BFLAF mutant streptavidin by addition of carbazole-labeled biotin.The fluorescence intensities of the Trp120BFLAF mutant streptavidin decreased as the concentration of carbazole-labeled biotin increased, and the fluorescence intensity was 1.4 times in the absence of carbazole-labeled biotin compared with that in the presence of carbazole-labeled biotin (100 nM).

(d) The fluorescence intensities of the Trp120BFLAF mutant streptavidins in the presence of various concentration of carbazole-labeled biotin at 510 m were plotted. Fluorescence intensity of Trp120BFLAF mutant streptavidin decreased linearly in the presence of carbazole-labeled biotin at the concentration range of 10 to 100 nM, and the quenching was saturated over 100 nM. All of the fluorescence spectra of mutant streptavidins were excited at 490nm.

For optimization of the spacer arm between biotin and carbazole, the carbazole-LC-biotin and carbazole-LC-LC-biotin were also synthesized, and the fluorescence quenching of Trp120BFLAF were examined upon addition with each of these compounds. The fluorescence spectra of Trp120BFLAF upon titration with carbazole-LC-biotin indicated that the fluorescence intensity was hardly any change (Fig.20a, b). But the fluorescence intensity of Trp120BFLAF was increased by addition of carbazole-LC-LC-biotin (Fig.20c, d). It is possibly because of the spacer of carbazole-labeled biotin when the carbazole-LC-biotin or carbazole-LC-LC-biotin bound to the Trp120BFLAF, and the conformational change of Trp120BFLAF would induce the increase of the fluorescence intensity of Trp120BFLAF. Also because of the spacer of carbazole-labeled biotin, in case of carbazole-LC-biotin, the increased fluorescence intensity by conformational change was quenched by carbazole, finally, apparently hardly any change of the fluorescence spectra of Trp120BFLAF upon titration with carbazole-LC-biotin was observed. But in case of carbazole-LC-LC-biotin, carbazole spatially detach from BFLAF which incorporated into the position of Trp120, and also the fluorescence quenching between these was difficult to occur.

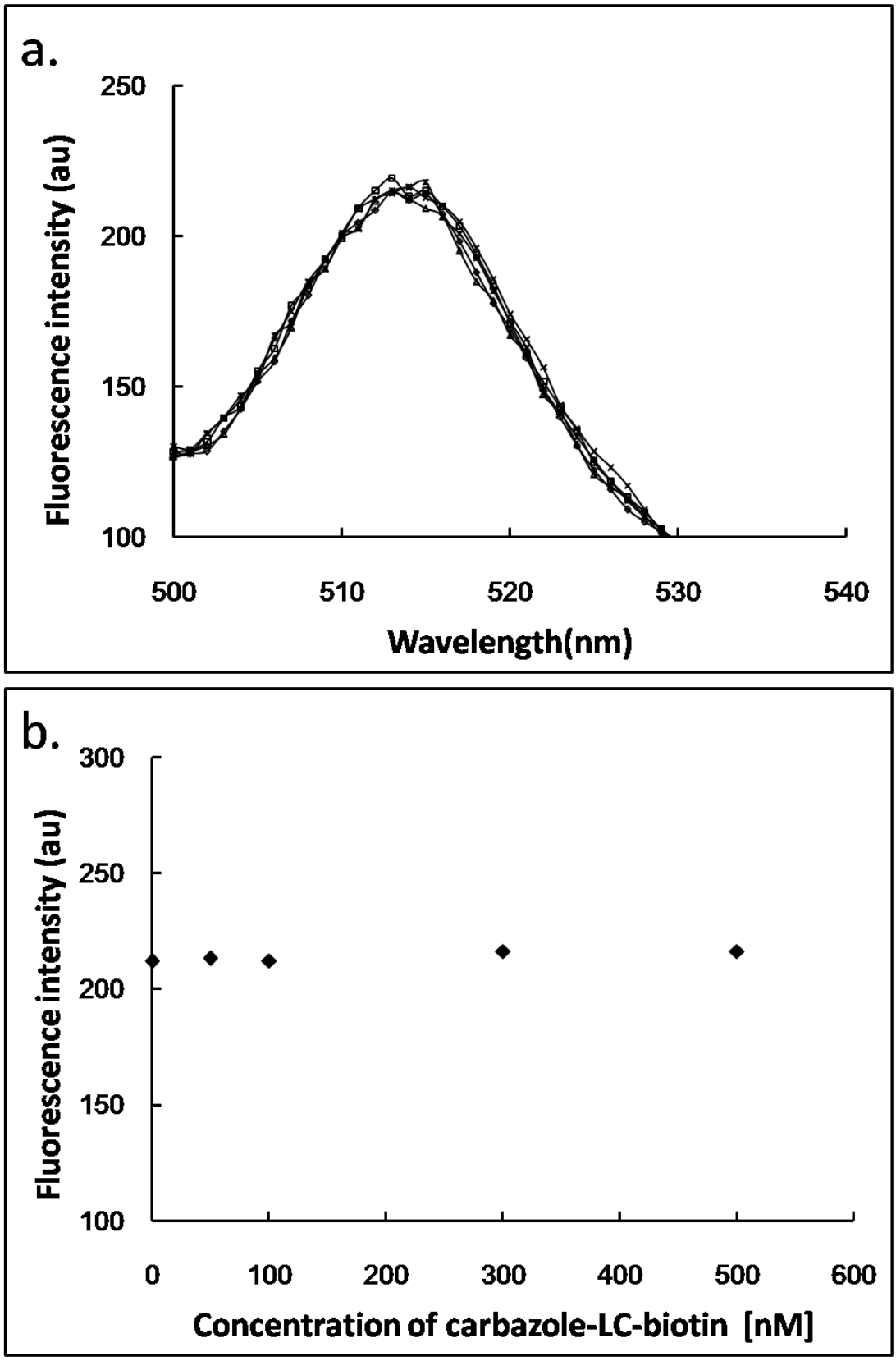
a.
Fluorescence intensity (au)
250
200
150
100
500
510
520
530
540
Wavelength(nm)
b.
Fluorescence intensity (au)
300
250
200
150
100
0
100
200
300
400
500
600
Concentration of carbazole-LC-biotin [nM]

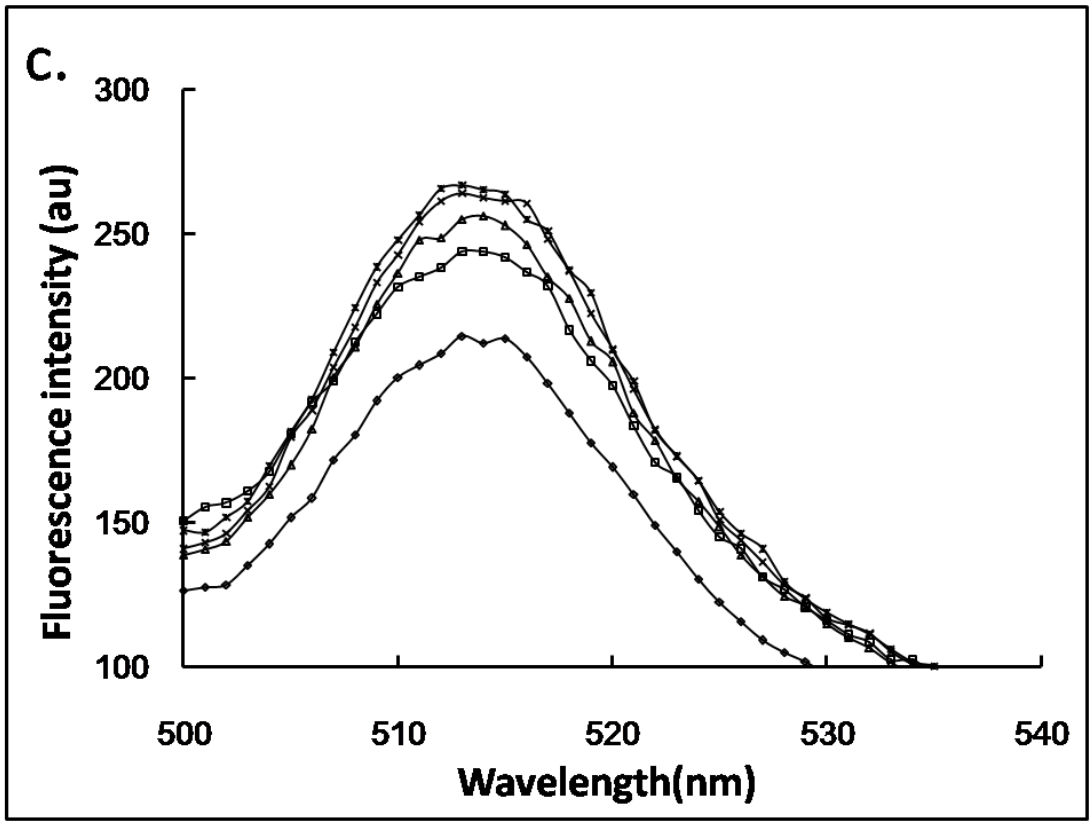
c.
300
250
200
150
100
Fluorescence intensity (au)
500
510
520
530
540
Wavelength(nm)

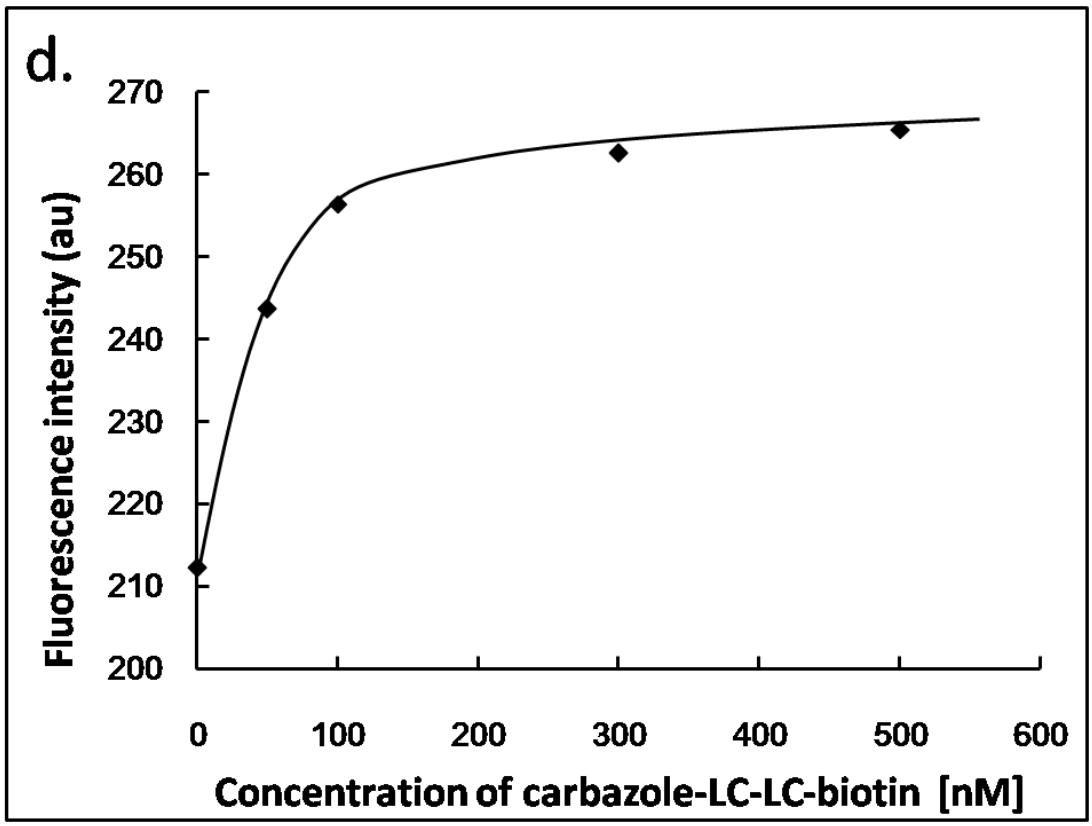
d.
270
260
250
240
230
220
210
200
Fluorescence intensity (au)
0
100
200
300
400
500
600
Concentration of carbazole-LC-LC-biotin [nM]

Fig.20 (a) (c) Fluorescence spectra of the Trp120BFLAF mutant streptavidin in the presence of 0 nM (—◇—), or 50 nM (—□—),or 100 nM (—△—), or 300 nM (—✕—), or 500 nM (—■—) of carbazole-LC-biotin(a) or carbazole-LC-LC-biotin(c).

(b) (d) The fluorescence intensities of the Trp120BFLAF mutant streptavidins in the presence of various concentration of carbazole-LC-biotin(b) or carbazole-LC-LC-biotin(d) at 510nm were plotted. All of the fluorescence spectra of mutant streptavidins were excited at 490nm.

Biotin sensing by measurement of fluorescence recovery of fluorescent mutant streptavidin and carbazole-labeled biotin system:

Finally, we applied the fluorescence quenching of the Trp120BFLAF mutant streptavidin by the binding of carbazole-labeled biotin to the molecular biosensing system for free biotin detection. Streptavidin has very high affinity to biotin, and then the streptavidin-biotin binding was almost irreversible. For accurate quantitative analysis of biotin, we determined the biotin concentration with the following two steps; (i) biotin was first added into the Trp120BFLAF mutant streptavidin solution, (ii) overdose of carbazole-labeled biotin was next added for binding to the mutant streptavidin solution. Fluorescence recovery of the Trp120BFLAF mutant streptavidin with carbazole-labeled biotin (100 nM) was observed upon the addition of natural biotin. Furthermore, biotin concentration dependent recovery of fluorescence intensity of the Trp120BFLAF mutant streptavidin with carbazole-labeled biotin (100 nM) upon competitive addition of biotin was observed (Fig.21). These results demonstrated that the fluorescence recovery by the couple of the fluorescent Trp120BFLAF mutant streptavidin and carbazole-labeled biotin was successfully applied for biotin sensing. Free biotin was determined in the concentration from 20 to 100 nM in this method.

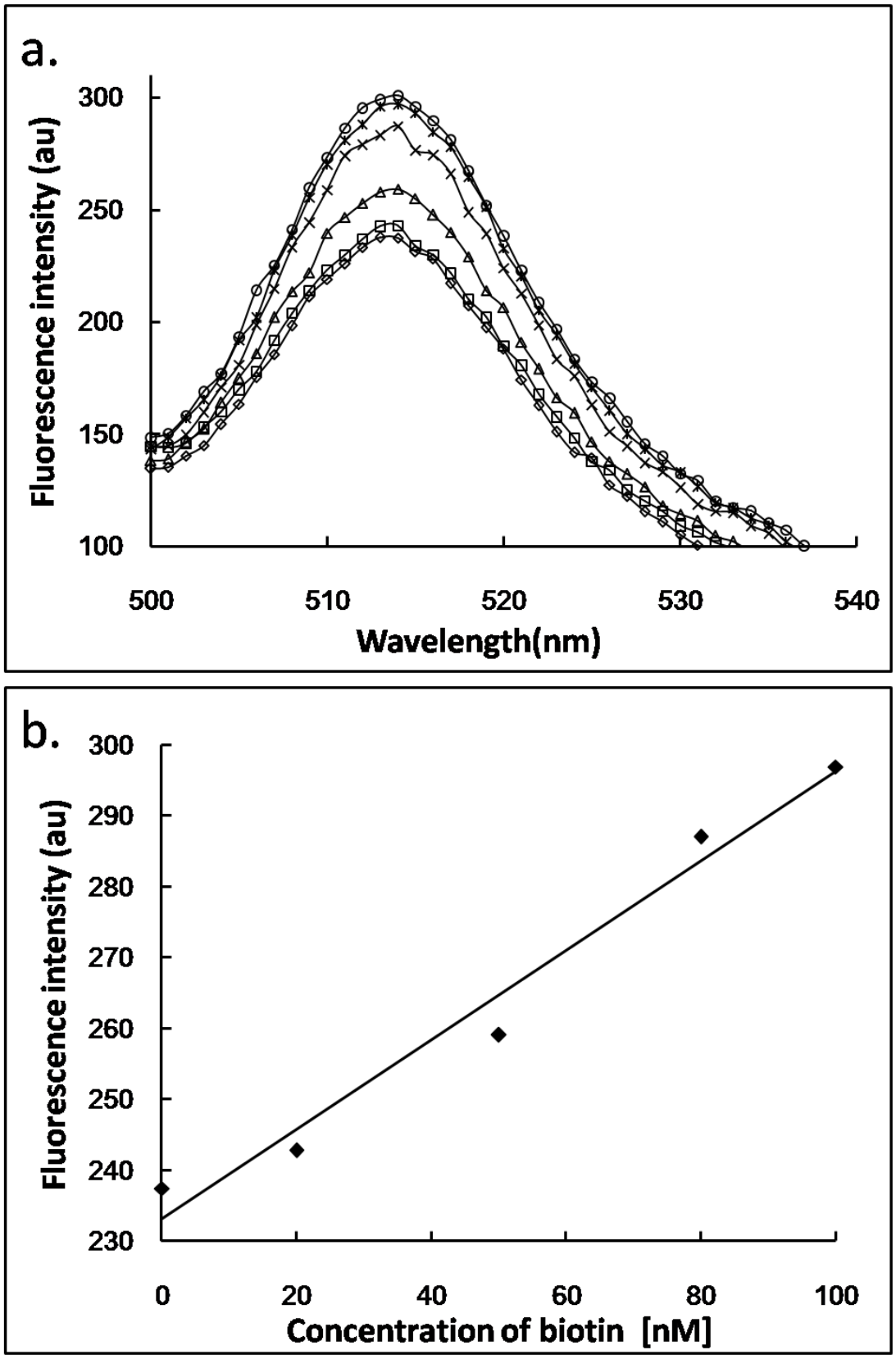
a.
Fluorescence intensity (au)
300
250
200
150
100
500
510
520
530
540
Wavelength(nm)
b.
Fluorescence intensity (au)
300
290
280
270
260
250
240
230
0
20
40
60
80
100
Concentration of biotin [nM]

Fig.21 (a) Fluorescence spectra of the Trp120BFLAF mutant streptavidin only (—O—) and in the presence of the pairs of 0 nM (—◇—), or 20 nM (—□—), or 50 nM (—△—), or 80 nM (—×—), or 100 nM (—✳—), of natural biotin and 100 nM of carbazole-labeled biotin. Fluorescence recovery of Trp120BFLAF mutant streptavidin quenched by carbazole-labeled biotin (100nM) was observed upon biotin addition.

(b) The fluorescence intensities of the Trp120BFLAF mutant streptavidins in the presence of various concentration of carbazole-labeled biotin at 510 m were plotted. Fluorescence quenching recovery by biotin addition depended on the concentration of free biotin. This result demonstrated fluorescence quenching recovery based biosensor for biotin was successfully fabricated with the combination of Trp120BFLAF mutant streptavidin and carbazole-labeled biotin. All of the fluorescence spectra of mutant streptavidins were excited at 490nm.

Chapter.3 Molecular biosensor for biotin base on Fluorescence enhancement of fluorescent unnatural mutant streptavidin by a biotin analogue with spacer tail

3.1 Introduction:

Tryptophan could quench the fluorescence from the fluorophore which was modified to the target protein at the position near the tryptophan was reported recently [23]. In this study, the BFLAF was incorporated into streptavidin at the Trp120 position with the four-base codon method. The synthesized and purified Trp120BFLAF mutant streptavidin showed fluorescence certainly as we expected. And the fluorescent mutant streptavidin had enough biotin binding activity as about 70% as wild type of streptavidin. We further discovered that fluorescence of the Trp120BFLAF mutant streptavidin was enhanced when the biotin analogue with a (AC5)2-hydrazide tail was bound to the fluorescent binding protein, whereas natural biotin binding did not induce the fluorescence intensity change. We then speculate that the fluorescence quenching of Trp120BFLAF by Trp79, Trp108 of the neighbor subunit may be disturbed by the long spacer tail of the biotin analogue. Finally, we applied this fluorescence enhancement of the Trp120BFLAF mutant streptavidin by binding of biotin-(AC5)2-hydrazide to the molecular biosensing system for free biotin based on the competitive binding reaction of free biotin and biotin-(AC5)2-hydrazide. Sensitive detection of free biotin was performed in the concentration range of 20 to 100 nM.

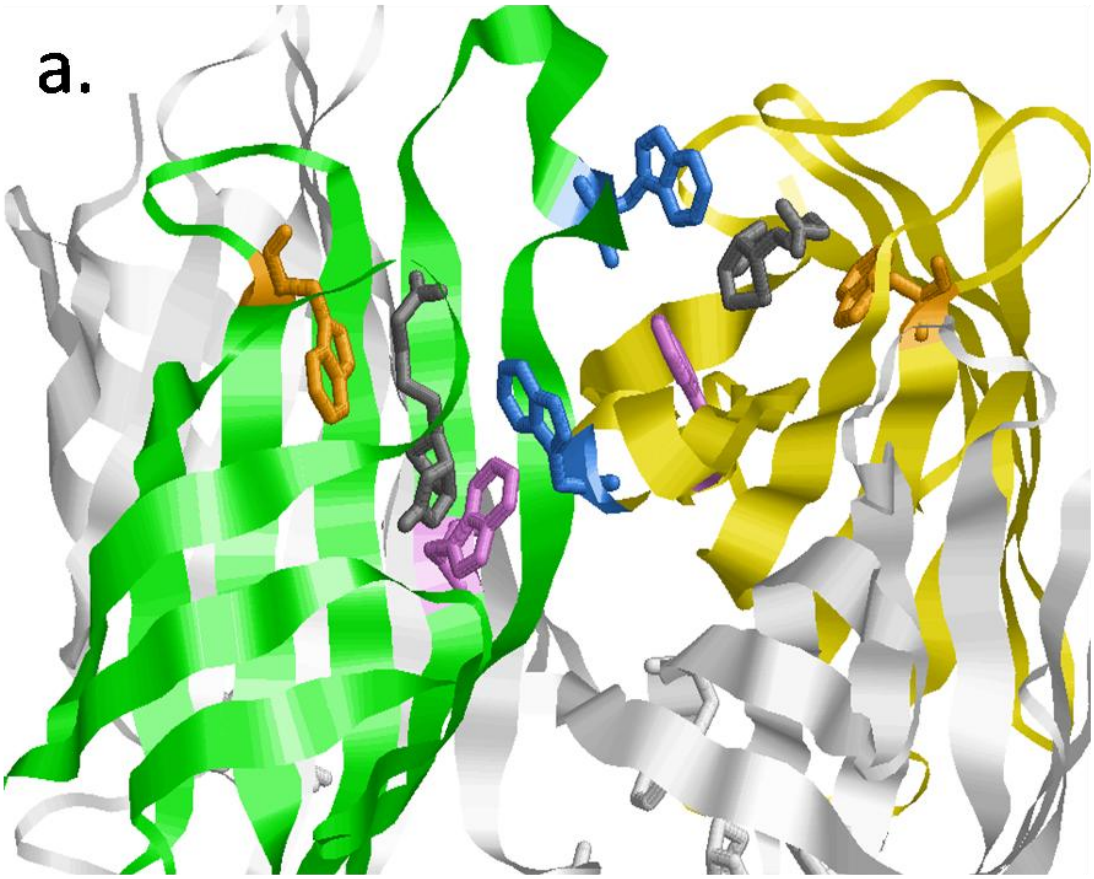

Fig.22 The homo tetrameric constitution of a natural streptavidin (PDB ID: 1SWE). Subunit A was colored with green, subunit B was colored yellow, for easy to see, both subunit C and D were colored with white. Biotin was colored with gray. On the other hand, Trp79, Trp108 and Trp120 in subunit A and B were colored with orange, violet and blue, respectively. Obviously the Trp120 was close to the Trp79 and the Trp108 of the neighbor subunit. (The distance between Trp120 to Trp79 of the neighbor subunit is 8.74Å and Trp120 to Trp108 of the neighbor subunit is 6.78Å.)

3.2 Experimental method:

3.2-1 Experimental procedure for fluorescence biosensing:

The biotin-$(AC_5)_2$-hydrazide was first dissolved in DMSO. 10 µl of the mutant streptavidin solution was mixed with 30 µl of the biotin-$(AC_5)_2$-hydrazide solution and 10 µl of the biotin solution, and then diluted to 100 µl with HKM buffer（100 mM KCl, 25 mM Hepes, 5 mM $MgCl_2$, pH adjusted to 7.4 with KOH). A fluorescence spectrometer (JASCO FP-6500) was used to measure excitation and emission spectra of the sample solutions with the slit width in 5 nm for both excitation and emission.

3.3 Result and discussion:

3.3-1 Fluorescence measure of the unnatural mutant streptavidins upon binding of biotin-$(AC_5)_2$-hydrazide and free biotin:

In this study, the biotin-$(AC_5)_2$-hydrazide was used as a biotin analogue with a long spacer tail in which the hydrazide group was inactive to protein, and the double of 6-aminohexanoic acid linker was expected to disturb the fluorescence quenching of the Trp120BFLAF by Trp79 or Trp108 of the neighbor subunit. Tyr83BFLAF was used as a contrast. Before the experiment of fluorescence enhancement of the fluorescent mutant streptavidin by the addition of biotin-$(AC_5)_2$-hydrazide, 100 nM of natural biotin was added into the solution of mutant streptavidins for confirming the no effect of natural biotin. Actually, the effect of fluorescence intensity from natural biotin was little (Fig.23a, b).

The Fluorescence spectra of fluorescent mutant streptavidins (Tyr83BFLAF and Trp120BFLAF) upon the addition with biotin-$(AC_5)_2$-hydrazide were next measured. There was almost no change in the fluorescence intensity of Tyr83BFLAF mutant streptavidin in the presence (100 nM) and absence of biotin-$(AC_5)_2$-hydrazide (Fig.23a).

In contrast, the Trp120BFLAF mutant streptavidin showed the marked fluorescence enhancement upon the addition of biotin-$(AC_5)_2$-hydrazide (100 nM). The fluorescence intensity of the Trp120BFLAF mutant streptavidin was 1.18 times higher than that in the absence of biotin-$(AC_5)_2$-hydrazide (100 nM) (Fig.23b). The fluorescence enhancement of Trp120BFLAF mutant streptavidin was observed upon the addition of 20 nM biotin-$(AC_5)_2$-hydrazide. Concentration dependence for fluorescence enhancement of Trp120BFLAF mutant streptavidin upon the addition of biotin-$(AC_5)_2$-hydrazide was shown in Fig.23c. Though this fluorescence enhancement of the Trp120BFLAF mutant streptavidin may be due to the disturbance of the fluorescence quenching of Trp120BFLAF by Trp79 or Trp108 of the neighbor subunit by the binding of biotin-$(AC_5)_2$-hydrazide with the long spacer tail as we expected, we did not have the direct evidence at the present stage. We will reconsider this mechanism for the fluorescence enhancement by the site-directed mutation of Trp79 and Trp108 in near future.

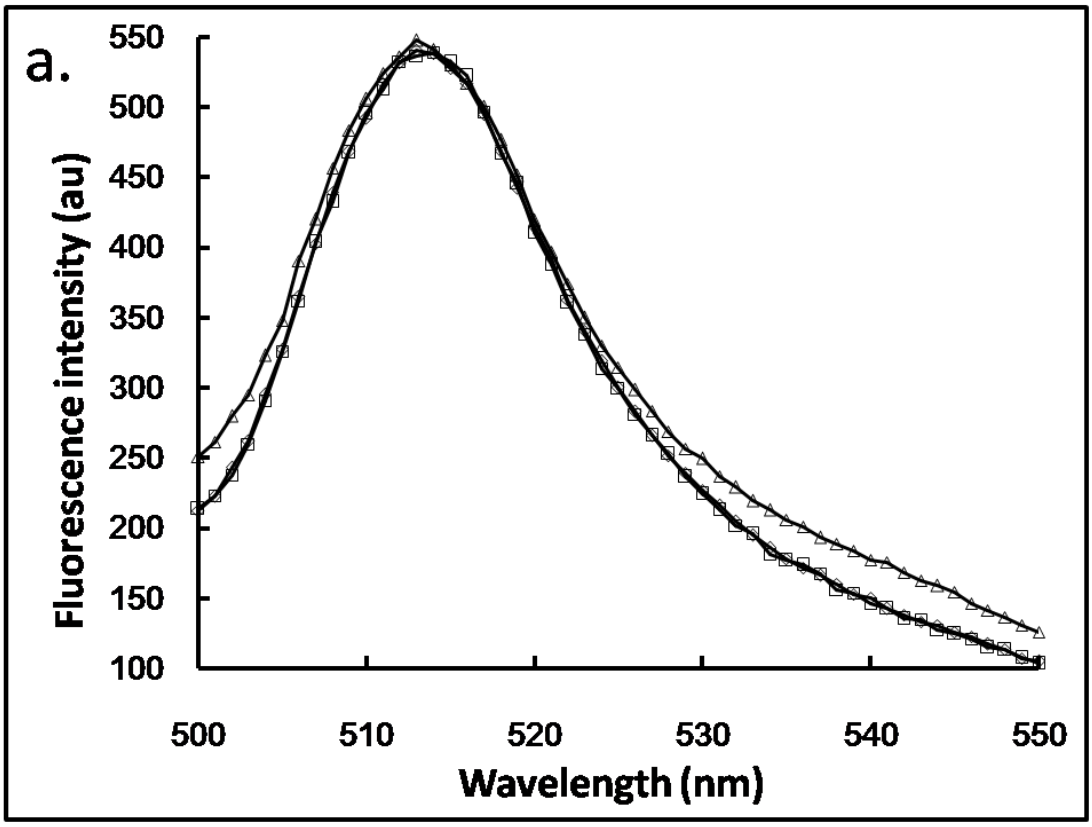
a.
Fluorescence intensity (au)
550
500
450
400
350
300
250
200
150
100
500
510
520
530
540
550
Wavelength (nm)

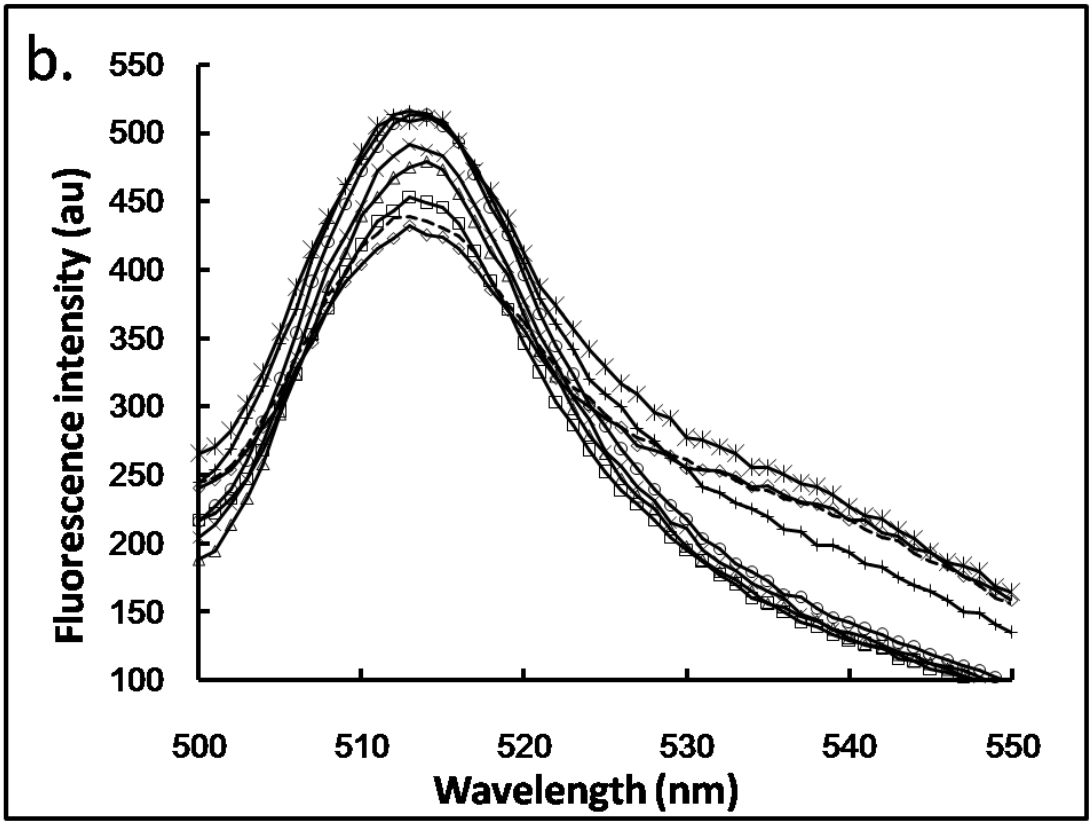
b.
Fluorescence intensity (au)
550
500
450
400
350
300
250
200
150
100
500
510
520
530
540
550
Wavelength (nm)

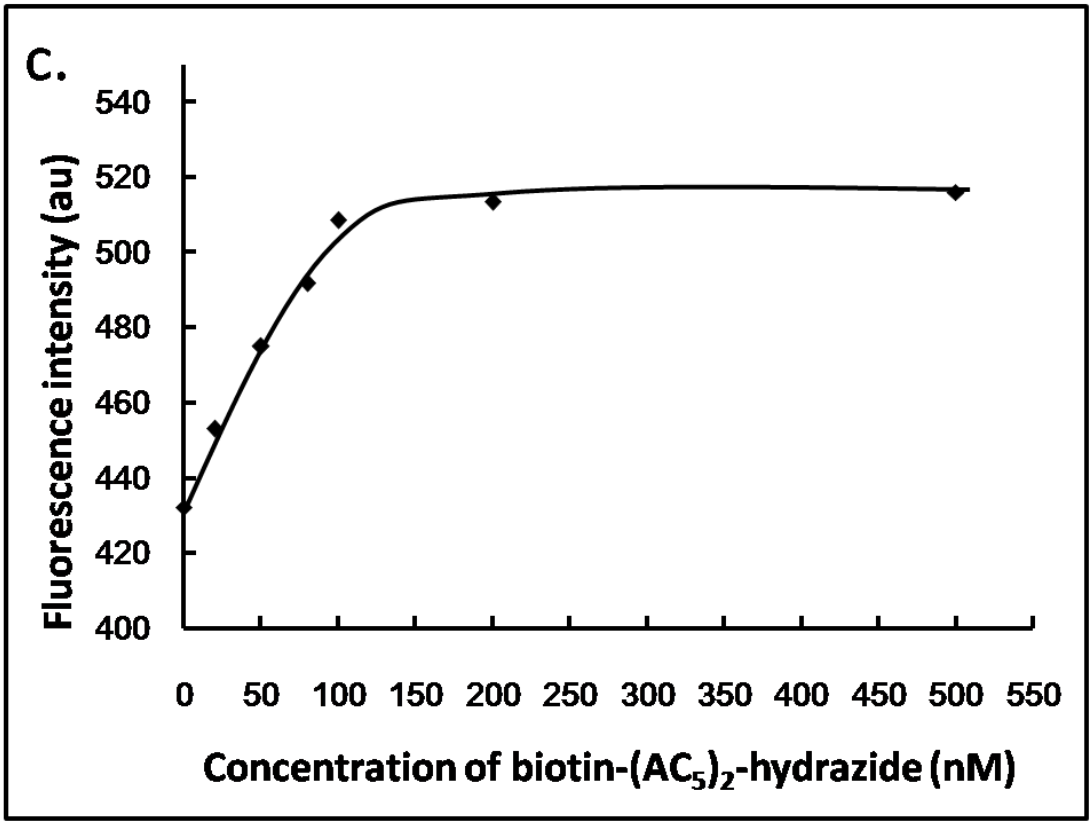

Fig.23 (a) Fluorescence spectrum of the Tyr83BFLAF mutant streptavidin only (—O—); Fluorescence spectrum of the Tyr83BFLAF mutant streptavidin in the presence of 100 nM of natural biotin (—Δ—) or 100 nM of biotin-$(AC_5)_2$-hydrazide (—□—); There was no change in the fluorescence intensity upon addition of natural biotin or biotin-$(AC_5)_2$-hydrazide for Tyr83BFLAF mutant streptavidin.

(b) Fluorescence spectra of the Trp120BFLAF mutant streptavidin only (—◇—), in the presence of 100 nM of biotin (·····), or 20 nM (—□—), or 50 nM (—Δ—), or 80 nM (—×—), or 100 nM (—✳—), or 200 nM (—O—), or 500 nM (—|—) of biotin-$(AC_5)_2$-hydrazide. Marked fluorescence enhancement was observed for the Trp120BFLAF mutant streptavidin by addition of biotin-$(AC_5)_2$-hydrazide.

(c) Dependence of the fluorescence enhancement of Trp120BFLAF mutant streptavidin on the concentration of added biotin-$(AC_5)_2$-hydrazide (20 nM to 100 nM) was observed. The fluorescence intensities of the Trp120BFLAF mutant streptavidins in the presence of various concentration of biotin-$(AC_5)_2$-hydrazide at 510nm were plotted. All of the fluorescence spectra of mutant streptavidins were excited at 490nm.

Finally, we applied the fluorescence enhancement of the Trp120BFLAF mutant streptavidin by the binding of biotin-$(AC_5)_2$-hydrazide to the molecular biosensing system for free biotin detection. Streptavidin has very high affinity to biotin, and then the streptavidin-biotin binding was almost irreversible. For accurate quantitative analysis of biotin, we determined the biotin concentration with the following two steps; (i) biotin was first added into the Trp120BFLAF mutant streptavidin solution, (ii) overdose of biotin-$(AC_5)_2$-hydrazide was next added for binding to the mutant streptavidin solution. Fluorescence decrease of the Trp120BFLAF mutant streptavidin with biotin-$(AC_5)_2$-hydrazide (100 nM) was observed upon the addition of natural biotin. Furthermore, biotin concentration dependent decrease of fluorescence intensity of the Trp120BFLAF mutant streptavidin with biotin-$(AC_5)_2$-hydrazide (100 nM) upon competitive addition of biotin was observed (Fig.24a, b). These results demonstrated that the fluorescence enhancement by the pair of the fluorescent Trp120BFLAF mutant streptavidin and biotin-$(AC_5)_2$-hydrazide was successfully applied for biotin sensing. Free biotin was determined in the concentration from 20 to 100 nM in this method.

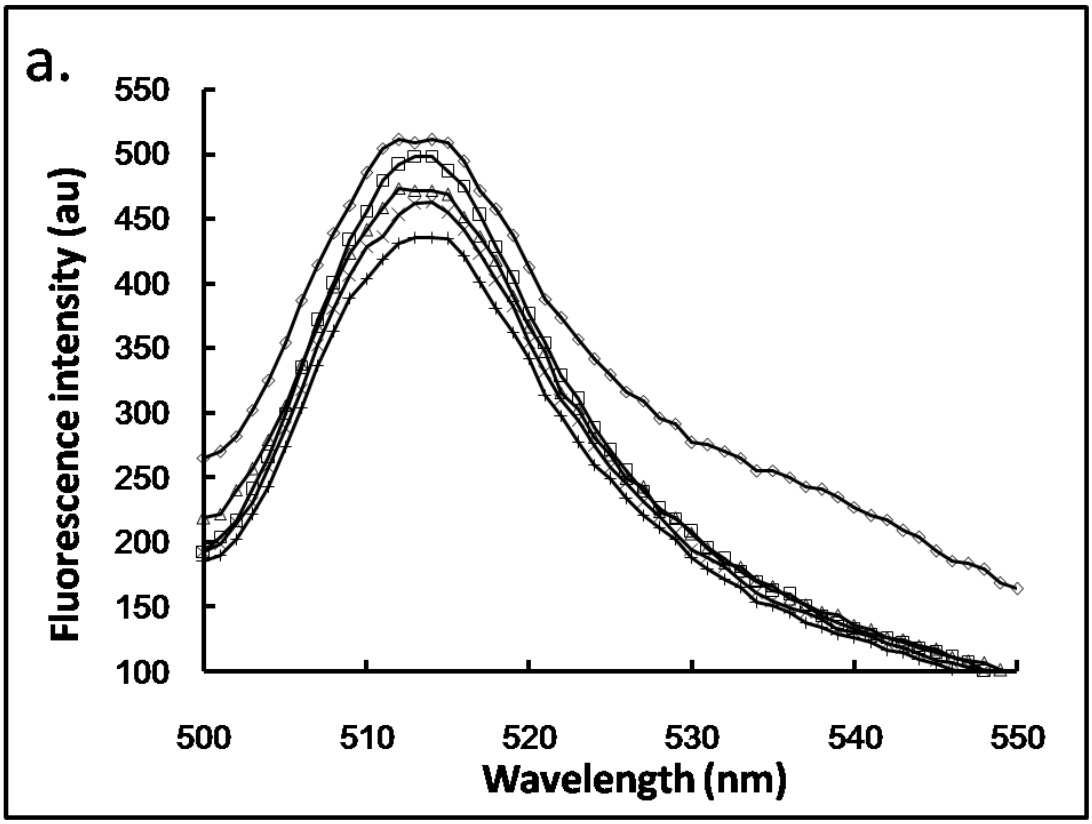
a.
Fluorescence intensity (au)
550
500
450
400
350
300
250
200
150
100
500
510
520
530
540
550
Wavelength (nm)

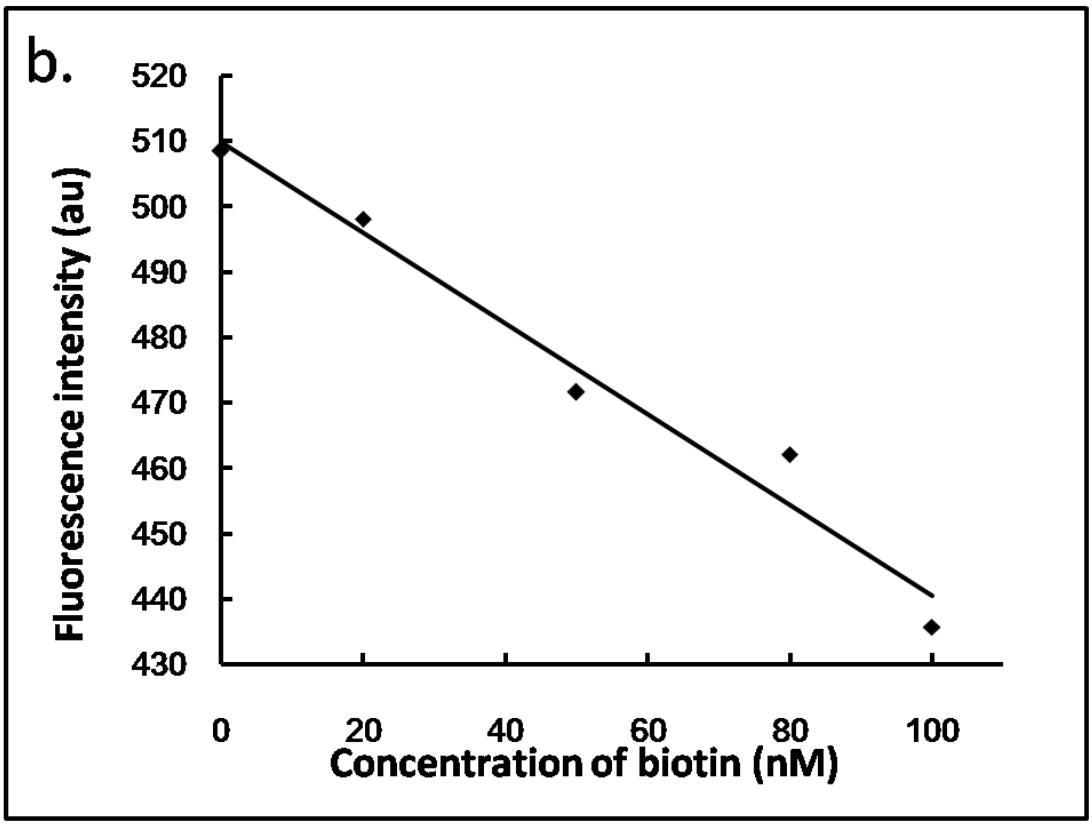
b.
Fluorescence intensity (au)
520
510
500
490
480
470
460
450
440
430
0
20
40
60
80
100
Concentration of biotin (nM)

Fig.24 (a) Fluorescence spectra of the Trp120BFLAF mutant streptavidin in the presence of the pairs of 0 nM (), or 20 nM (), or 50 nM (), or 80 nM (), or 100 nM (), of natural biotin and 100 nM of biotin-$(AC_5)_2$-hydrazide. Marked fluorescence enhancement was observed for the Trp120BFLAF mutant streptavidin by addition of biotin-$(AC_5)_2$-hydrazide. Decrease of fluorescence of Trp120BFLAF mutant streptavidin was observed upon competitive biotin addition in the presence of 100nM of biotin-$(AC_5)_2$-hydrazide.

(b) The fluorescence intensities of the Trp120BFLAF mutant streptavidins in the presence of the pairs of various concentrations of natural biotin and 100 nM of biotin-$(AC_5)_2$-hydrazide at 510nm were plotted. Fluorescence intensity of the Trp120BFLAF mutant streptavidin depended on the concentration of free biotin. All of the fluorescence spectra of mutant streptavidins were excited at 490nm.

Chapter.4 Conclusion and Perspective:

In this study, two types of new molecular biosensor for biotin were developed. The two types of molecular biosensor for biotin were realized because of a rigorous design to make artificial protein by using four-base codon method. These results suggested molecular biosensor for small ligand could be successfully designed in the couple of genetically engineered fluorescent mutant binding protein and quencher-labeled ligand analogue. And also it suggested that molecular biosensor for small ligand could be successfully designed in the pair of genetically engineered fluorescent mutant binding protein and ligand analogue.

Acknowledgments:

研究論文を作成するにあたり終始多大なるご助言、ご指導をいただきました、富山大学工学部　篠原寛明教授に厚く御礼申し上げます。

また、副査として論文審査を通して本研究論文作成にあたり助言をいただいた、富山大学工学部　磯部正治教授に厚く感謝申し上げます。

また、副査として論文審査を通して本研究論文作成にあたり助言をいただいた、富山大学工学部　北野博巳教授に厚く感謝申し上げます。

また、本研究遂行にあたり技術指導、有益なご助言をいただきました、富山大学工学部須加助教に厚く感謝申し上げます。

また、本研究遂行にあたり試薬の供給、有益なご助言をいただきました、共同研究先である北陸先端科学技術大学院大学　芳坂貴弘教授に厚く感謝申し上げます。

また、本研究遂行にあたり技術指導、有益なご助言をいただきました、富山大学工学部　黒田重靖教授に厚く感謝申し上げます。

また、本研究遂行にあたり技術指導、有益なご助言をいただきました、富山大学工学部　宮武滝太准教授に厚く感謝申し上げます。

また、本研究遂行にあたり技術指導、ご助言をいただきました、共同研究先である北陸先端科学技術大学院大学　芳坂研究室の皆様方に深く感謝申し上げます。

最後に研究ディスカッションや励ましをいただいた篠原研究室の先輩方、後輩の皆さんに感謝いたします。

References:

[1] Kuhlman, Brian. Dantas, Gautam. Ireton, Gregory C. Varani, Gabriele. Stoddard, Barry L. Baker, David. "Design of a Novel Globular Protein Fold with Atomic-Level Accuracy" *Science*, **302,** 1364–1368 (2003).

[2] Loren L. Dwyer, Mary A. Smith, James J. Hellinga, Homme W. "Comp utational design of receptor and sensor proteins with novel functions" *Nature*, **423**, 185–190 (2003).

[3] Khoury,GA. Fazelinia, H. Chin, JW. Pantazes, RJ. Cirino, PC. Maranas,CD. "Computational design of Candida boidinii xylose reductase for altered cofactor specificity" *Protein Science,* **18,** 2125–2138 (2009).

[4] Ardejani, MS. Li, NX. Orner, BP. "Stabilization of a Protein Nanocage through the Plugging of a Protein–Protein Interfacial Water Pocket" *Biochemistry,* **50,** 4029–4037 (2011).

[5] D. Adlercreutz, P. Tufvesson, A. Karlsson, R. Hatti-Kaul. "Alkonolamide biosurfactants: techno-economic evaluation of biocatalytic versus chemical production" *Ind. Biotechnol,* **6**, 204–211 (2010).

[6] J. Andraos. "Safety/hazard indices: completion of a unified suite of metrics for the assessment of 'Greeness' for chemical reactions and synthesis plans" *Org. Proc. Res. Dev.,* **17**, 175–192 (2013).

[7] U.T. Bornscheuer, G.W. Huisman, R.J. Kazlauskas, S. Lutz, J.C. Moore, K. Robins. "Engineering the third wave of biocatalysis" *Nature,* **485,** 185–194 (2012).

[8] J.J. Bozell, G.R. Petersen. "Technology development for the production of biobased products from biorefinery carbohydrates—the US Department of Energy's Top 10 revisited" *Green Chem.,* **12,** 539–554 (2010).

[9] Z. Zhu, M. Wang, A. Gautam, J. Nazor, C. Momeu, R. Prodanovic, U. Schwaneberg. "Directed evolution of glucose oxidase from *Aspergillus niger* for ferrocenemethanol-mediated electron transfer" *Biotechnol. J.,* **2,** 241–248 (2007).

[10] C.F.B. Witteveen, P. van da Vordervoort, K. Swart, J. Visser. "Glucose oxidase overproducing and negative mutants of *Aspergillus niger" Appl. Microbiol. Biotechnol.,* **33,** 683–686 (1990).

[11] S. Nagayama, S. Zeng, W. Xiong, M.L. Fletcher, A.V. Masurkar, D.J. Davis, V.A. Pieribone, R.W. Chen. "*In vivo* simultaneous tracing and Ca^{2+} imaging of local neuronal circuits" *Neuron,* **53,** 789–803 (2007).

A. Miyawaki, J. Llopis, R. Heim, J.M. McCaffery, J.A. Adams, M. Ikura, R.Y. Tsien. "Fluorescent indicators for Ca^{2+} based on green fluorescent proteins and calmodulin" *Nature,* **388,** 882–887 (1997).

[12] Hohsaka T, Sate K, Sisido M, Takaib K, Yokoyamaba S. "Site-specific incorporation of photofunctional nonnatural amino acids into a polypeptide through in vitro protein biosynthesis" *FEBS Letters,* **344,** 171-174 (1994).

[13] Kanda T, Takai K, Hohsaka T, Sisido M, Takaku H. Sense. “Codon-Dependent Introduction of Unnatural Amino Acids into Multiple Sites of a Protein” *Biochemical and Biophysical Research Communications,* **270,** 1136–1139 (2000).

[14] Hohsaka T, Sisido M. “Incorporation of non-natural amino acids into proteins” *Current Opinion in Chemical Biology,* **6,** 809–815 (2002).

[15] yamanaka K, Nakata H, Hohsaka T, Sisido M. “Efficient Synthesis of Nonnatural Mutants in Escherichia coli S30 in vitro Protein Synthesizing System” *Journal of Bioscience and Bioengineering,* **97,** 395-399 (2004).

[16] Hohsaka T, Muranaka N, Komiyama C, Matsui K, Takaura S, Abe R, Murakami H, Sisido M. “Position-specific incorporation of dansylated non-natural amino acids into streptavidin by using a four-base codon” *FEBS Letters,* **560,**173-177 (2004).

[17] Taira H, Fukushima M, Hohsaka T, Sisido M. “Four-Base Codon-Mediated Incorporation of Nonnatural Amino Acids into Proteins in a Eukaryotic Cell-Free Translation System” *Journal of Bioscience and Bioengineering,* **99,** 473-476 (2005).

[18] Turner, Anthony; Wilson, George and Kaube, Isao (eds.). *Biosensors:Fundamentals and Applications*. Oxford, UK: Oxford University Press. 770 (1987).

[19] Bănică, Florinel-Gabriel. *Chemical Sensors and Biosensors:Fundamentals and Applications*. Chichester, UK: John Wiley & Sons. 576 (2012).

[20] Cavalcanti A. Shirinzadeh B. Zhang M. Kretly LC. "Nanorobot Hardware Architecture for Medical Defense" *Sensors,* **8,** 2932–2958 (2008).

[21] M. Iqbal, M. A. Gleeson, B. Spaugh, F. Tybor, W. G. Gunn, M. Hochberg, T. Baehr-Jones, R. C. Bailey, L. C. Gunn, "Label-Free Biosensor Arrays Based on Silicon Ring Resonators and High-Speed Optical Scanning Instrumentation" *IEEE J. Sel. Top. Quant. Elec.,* **16,** 654-661 (2010)

[22] J. Witzens, M. Hochberg. "Optical detection of target molecule induced aggregation of nanoparticles by means of high-Q resonators" *Opt. Express,* **19,** 7034–7061 (2011).

[23] Fan, F. et al. “Novel Genetically Encoded Biosensors Using Firefly Luciferase” *ACS Chem. Biol.,* **3,** 346–51 (2008).

[24] Phillips SR, Wilson LJ, Borkman RF.“Acrylamide and iodide fluorescence quenching as a structural probe of tryptophan microenvironment in bovine lens crystallins” *Curr Eye Res*., **5,** 611-619 (1986).

[25] James E. O'Reilly. “Fluorescence experiments with quinine” *J. Chem. Educ*., **52,** 610 (1976).

[26] LouAnn Sacksteder , R. M. Ballew , Elizabeth A. Brown , J. N. Demas , D. Nesselrodt and B. A. DeGraff . “Photophysics in a disco: Luminescence quenching of quinine” *J. Chem. Educ.,* **67,** 1065 (1990).

[27] Jonathan H. Gutow. “Halide (Cl-) Quenching of Quinine Sulfate Fluorescence: A Time-Resolved Fluorescence Experiment for Physical Chemistry” *J. Chem. Educ.*, **82,** 302 (2005).

[28] Peng, X. Chen, H. Draney, D.R. Volcheck, W.M. “A Non-fluorescent, Broad Range Quencher Dye for FRET Assays”, *Analytical Biochemistry*, **388,** 220–228 (2009).

[29] Blum G, Weimer RM, Edgington LE, Adams W, Bogyo M. “Comparative Assessment of Substrates and Activity Based Probes as Tools for Non- Invasive Optical Imaging of Cysteine Protease Activity”. **4,** 6374 (2009).

[30] Weissleder R, Tung CH, Mahmood U, Bogdanov A. "In vivo imaging of tumors with protease-activated near-infrared fluorescent probes". *Nat. Biotechnol.,* **17,** 375–378 (1999).

[31] Hardinge MG, Crooks H. “Lesser known vitamins in foods” *Journal of the American Dietetic Association,* **38,** 240-244 (1960).

[32] Hoppner K, Lampi B. Total folate, “pantothenic acid and biotin content of yogurt products” *Canadian Institute of Science and Technology Journal,* **23,** 223-225 (1992).

[33] Zempleni J, Mock DM. “Biotin biochemistry and human requirements” *J. Nutr. Biochem,* **10,** 128 –138 (1999).

[34] Staggs CG, Sealey WM, McCabe BJ, Teague AM, Mock DM. “Determination of thebiotin content of select foods using accurate and sensitive HPLC/avidin binding” J*ournal of Food Composition and Analysis,* **17,** 767-776 (2004).

[35] Pacheco-Alvarez D, Sergio Solórzano-Vargas R, león Del río A. “Biotin in Metabolism and Its Relationship to Human Disease” *Archives of Medical Research,* **33,** 439-447 (2002).

[36] Cornish VW, Mendel D, Schultz PG. “Probing Protein Structure and Function with an Expanded Genetic Code” *Angew. Chem. Int. Ed. Engl,* **34,** 621-633 (1995).

[37] Arslan T, Mamaev SV, Mamaeva NV, “Hecht SM Structurally Modified Firefly Luciferase. Effects of Amino Acid Substitution at Position 286” *American Chemical Society,* **119,** 10877-10887 (1997).

[38] Wang BX, Brown KC, Lodder M, Craik CS, Hecht SM. “Chemically Mediated Site-Specific Proteolysis. Alteration of Protein-Protein Interaction” *Biochemistry,* **41,** 2805-2813 (2002).

[39] Beene DL, Dougherty DA. Lestery HA Lestery, “Unnatural amino acid mutagenesis in mapping ion channel function” *Current Opinion in Neurobiology,* **13,** 264–270 (2003).

[40] Tausig F, Wolf FJ. “Streptavidin-a substance with avidin-like properties produced by microorganisms” *Biochemical and biophysical research communications,* **14,** 205-209 (1964).

[41] Chalet L, Wolf PJ. “The Properties of Streptavidin, a Biotin-Binding Protein Produced by Streptomycefes” *Archives of Biochemistry and Biophysics,* **106,** 1-5 (1964).

[42] Hendrickson WA, Pahler A, Smith JL, Satow Y, Merritt EA, “Phizackerley RPCrystal structure of core streptavidin determined from multiwavelength anomalous diffraction of synchrotron radiation” *Proc. Nati. Acad Sci USA,* **86,** 2190-2194 (1989).

[43] Kim TW, Yoon HY, Park JH, Kwon OH, Jang DJ, Hong JI. “Molecular Tripods Showing Fluorescence Enhancement upon Binding to Streptavidin” *Organic letters,* **7,** 111-114 (2005).

[44] Brown HC, Heydkamp WR, Breuer E, Murphy WS. “The Reaction of Organoboranes with Chloramine and with Hydroxylamine-O-sulfonic Acid. A Convenient Synthesis of Amines from Olefins via Hydroboration” *Journal of the American Chemical Society,* **86,** 3565-3566 (1964).

[45] Hoppner K, Lampi B. “Biotin content of cheese products” *Food Research International,* **25,** 41-43 (1992).